

# **Climate Assessment Report (CAR) – Comparison and evaluation of global tropospheric column ozone climatological means: Variability and trends (v1.0, 16 May 2024)**

Martin Dameris<sup>1</sup>, Klaus-Peter Heue<sup>2</sup>, Viktoria Sofieva<sup>3</sup>, Patrick Jöckel<sup>1</sup>, Moritz Witt<sup>1</sup>

<sup>1</sup> Deutsches Zentrum für Luft- und Raumfahrt, Institut für Physik der Atmosphäre, Oberpfaffenhofen, Germany

<sup>2</sup> Deutsches Zentrum für Luft- und Raumfahrt, Institut für Methodik der Fernerkundung, Oberpfaffenhofen, Germany

<sup>3</sup> Finnish Meteorological Institute, Space and Earth Observation Centre, Finland

## **Abstract**

This Climate Assessment Report (CAR) of ESA's Ozone\_cci+ project focuses on tropospheric ozone, in particular comparing different global climatologies (i.e. climatological means based on longer time periods), evaluating spatiotemporal variability of ozone in the troposphere as well as analysing long-term trends. For this, respective ozone data sets have been compared. The compilation of the findings presented and discussed in this report is based on currently available long-term ozone data series, including those prepared within the framework of the ESA Ozone\_cci project, which are based on multi-year observations from space-based instruments. In addition, multi-decadal simulations of Chemistry-Climate Models (CCMs) are used to support the respective analyses and help verify and classify the results. The evaluation of the different data sets shows clearly that the derived global distributions of tropospheric ozone are differing in detail. For the observational data, one possible reason for that is that the applied retrieval methods to derive the corresponding ozone data products are using different requirements and preliminary information or other boundary conditions, which strongly affect the data. In addition, the creation of consistent time series for longer periods (years to decades) represents a challenge because the used observations originate from different measuring systems. However, such long-term data sets are necessary to allow the derivation of robust trend estimates. Moreover, the identification of statistically significant trends is hard because the natural (internal) tropospheric ozone fluctuations are relatively large in comparison with the expected long-term changes of the tropospheric ozone content. Therefore, the determined tropospheric ozone trends are often depending on the length of the analysed period. Nevertheless, it follows from our study that robust trends can be identified in some regions, especially in the (sub-) tropics. In this context, results from multi-year simulations of CCMs can support the evaluation of the tropospheric ozone data products derived from measurements, for instance by disclosing obvious errors and thus helping to reduce the range of uncertainties.

Finally, to update the last CAR (Dameris et al., 2022), a short summary of the most important results of the current "WMO Scientific Assessment of Ozone Depletion: 2022" (WMO, 2022) is presented.

## **1. Introduction**

The International Global Atmospheric Chemistry Project (IGAC) created in recent years the Tropospheric Ozone Assessment Report (TOAR; [www.igacproject.org/activities/TOAR](http://www.igacproject.org/activities/TOAR)). The assessment report is organized as a series of scientific peer-reviewed papers. Among others, they

contain overviews about the current knowledge of the global tropospheric ozone distribution and trends. TOAR is an important basis for comparing and classifying new tropospheric ozone data sets, in this case the data products developed in the ESA Ozone\_cci project.

Global observations over several years (decades) derived from ground-, airborne- and satellite-based measuring systems are available (e.g., Gaudel et al., 2018; Tarasick et al., 2019; Wang et al., 2022). The determined tropospheric column ozone (TCO3) data sets often differ significantly, which is partly due to the fact that the algorithms used for the creation of the respective (level 1, 2 or 3) data products (i.e. calibration and retrieval algorithms, assumptions made, prior information) are themselves sometimes very different. Another challenge is the creation of consistent longer data series from different data sources (e.g. different instruments), which certainly makes it difficult to derive suitable longer data series allowing robust trend estimates.

The TOAR surface ozone data base (Schultz et al., 2017) considers adequately tested series of measurements, which provide information of tropospheric ozone, for instance derived from ground-based Fourier Transform Infrared (FTIR) or lidar instruments, through measurements with Dobson and Brewer spectrometers and ozonesondes. For instance, ozonesonde measurements are collected worldwide (see for example the World Ozone and Ultraviolet Radiation Data Centre, WOUDC, available at <https://woudc.org/data.php>). They contain ozone profile information from the surface up to about 35 km.

Furthermore, the data aircraft observations from the In-service Aircraft for a Global Observing System database (IAGOS) provide additional important information about the tropospheric ozone distribution since 1994 (Wang et al., 2022).

TOAR also includes tropospheric ozone data, which have been measured by satellite-borne instruments since 1995, for instance, by OMI (Ozone Monitoring Instrument), TROPOMI (TROPOspheric Monitoring Instrument), MLS (Microwave Limb Sounder), GOME/GOME-2 (Global Ozone Monitoring Experiment), IASI (Infrared Atmospheric Sounding Interferometer), OSIRIS (Optical Spectrograph and InfraRed Imaging System), MIPAS (Michelson Interferometer for Passive Atmospheric Sounding), SCIAMACHY (SCanning Imaging Absorption SpectroMeter for Atmospheric CHartography), OMPS-LP (Ozone Mapping and Profiles Suite – Limb Profiler), and GOMOS (Global Ozone Monitoring by Occultation of Stars). To make these measured (raw) data usable accordingly for scientific purposes, different retrieval algorithms have been applied to the original data, in most cases to derive TCO3 products.

Overall, this means that sometimes very different results are obtained. The aim is to uncover and eliminate errors and reduce uncertainties.

On the other hand, long-term (decadal) Chemistry-Climate Model (CCM) simulations were created (e.g. around the Chemistry-Climate Model Initiative (CCMI) supported by the WCRP SPARC project, among others accompanied for the WMO scientific ozone assessments) representing the past decades, which also contain different specifications and assumptions (e.g. the spatial resolution of the CCMs, use of different parameterisations, or the use of different emission inventories). These model-based data sets enable a direct comparison with respective values derived from observations. It offers the possibility to identify obvious similarities and major differences of the data record used, i.e. allowing a more robust evaluation (bench mark) of the available data, for instance to quantify the range of uncertainties.

The main objective of ESA-CCI is to provide reliable long-term Climate Data Records (CDRs), which are essential to assess the state and evolution of global climate. The aim of the Ozone\_cci project is to assemble consistent ozone data sets based on European satellite instruments that have been in

operation since the mid-1990s. An important contribution to the ESA Ozone\_cci+ project (second phase of the project) is the determination of tropospheric ozone trends, in particular looking at the appropriate data products derived from long-term measurements of the European satellite instruments. For this purpose, in a first step the derived global mean TCO<sub>3</sub> distributions in Ozone\_cci are compared and evaluated qualitatively and quantitatively with already existing (i.e. published in peer-reviewed journals) TCO<sub>3</sub> climatological mean distributions. Furthermore, they are compared with corresponding results from multi-decadal Chemistry-Climate Model (CCM) simulations. Long-term changes are then derived and evaluated on this basis. Similarities and differences are identified and discussed, allowing a classification of the trend statements.

As mentioned by Tarasick et al. (2019), as part of the TOAR, “the lack of information on temporal changes of biases for satellite measurements of tropospheric ozone is an area of concern for long-term trend studies”. Therefore, independent analyzes of the available tropospheric ozone data sets are necessary to get a clearer picture of the spatiotemporal fluctuations of tropospheric ozone and its long-term changes. The tropospheric ozone products created and examined in the frame of the ESA Ozone\_cci project are another corner stone for such research. The results derived from the CCM simulations can also be used here as a support. If the used CCMs are well established and verified and if such CCMs are driven with observed meteorology (i.e. reanalyses), their results should represent the “reality”. The differences of the simulation results and data sets derived from observations can be taken to estimate the range of uncertainty.

In the following section (Sec. 2) the used ESA ozone data products and methods how to derive them are briefly described as well as the used CCM EMAC. In Section 3 TCO<sub>3</sub> climatological means are discussed and compared. Sections 4 and 5 presents respective trend analyses of ESA related data sets and how they compare with other TCO<sub>3</sub> data products published so far. Section 6 provides a summary discussion of our findings and some final remarks. Finally, Section 7 briefly summarizes the most important statements from the last WMO scientific assessment of ozone depletion (WMO, 2022).

## **2. TCO<sub>3</sub> developed in the framework of ESA Ozone\_cci based on measurements and climate model simulations**

- The SUNLIT-OMI-LIMB data set

A tropospheric column ozone (TCO<sub>3</sub>) dataset has been created using a combination of total ozone columns from OMI (Ozone Monitoring Instrument) and TROPOMI (TROPOspheric Monitoring Instrument) with stratospheric ozone column datasets from several available limb-viewing instruments: MLS (Microwave Limb Sounder), OSIRIS (Optical Spectrograph and InfraRed Imaging System), MIPAS (Michelson Interferometer for Passive Atmospheric Sounding), SCIAMACHY (SCanning Imaging Spectrometer for Atmospheric CHartographY), OMPS-LP (Ozone Mapping and Profiles Suite – Limb Profiler), and GOMOS (Global Ozone Monitoring by Occultation of Stars). A detailed description of the SUNLIT (Synergy of Using Nadir and Limb Instruments for Tropospheric Ozone Monitoring) tropospheric ozone column product SUNLIT-OMI-LIMB TCO<sub>3</sub>, which is globally available from 2005 – 2019, is given by Sofieva et al. (2022). The TCO<sub>3</sub> dataset used here has a 1° × 1° horizontal resolution, from the surface up to 3 km below the tropopause, providing monthly-averaged TCO<sub>3</sub> values.

- T<sub>TOC</sub>\_CCD (= Convective Cloud Differential data) climate product

The tropical tropospheric column ozone (TTCO<sub>3</sub>) has been retrieved with the convective cloud differential (CCD) method. The CCD method retrieves the TCO<sub>3</sub> as the difference between total

column ozone and the stratospheric column ozone (SCO3). It utilizes the processed total ozone columns and cloud data as retrieval input. A description of the method how to create the TTOC\_CCD product is presented by Heue et al. (2016).

The TTCO3 data set covers the tropical belt from 20°N – 20°S in the years from 1995 – 2022, i.e. using information from GOME/GOME2, SCIAMACHY, OMI, and TROPOMI (monthly averages on a 1° × 1° (latitude × longitude)). CCD algorithms rely on total ozone and cloud data; both are taken from GODFITv4 data, available in ESA's Ozone\_cci. The average cloud top pressure for deep convective clouds is about 270 hPa (≈ 10 km). We used a climatology for harmonizing the above-cloud column ozone for different cloud altitudes.

- RAL Space UV-Vis satellite ozone products for the lower troposphere

Pope et al. (2023) investigated long-term spatiotemporal variability in lower tropospheric column ozone (LTCO3, surface – 450 hPa sub-column) by merging and harmonizing the multiple European Space Agency – Climate Change Initiative (ESA-CCI) products produced by the Rutherford Appleton Laboratory (RAL). Four RAL UV-Vis satellite products investigated were from OMI, the Global Ozone Monitoring Experiment (GOME), GOME-2 and the SCanning Imaging Absorption spectroMeter for atmospheric Cartography (SCIAMACHY), all of which were developed as part of the Ozone\_cci project. The RAL products cover the full period between 1996 and 2017.

- The RD1SD simulation from the CCM EMAC

The Chemistry-Climate Model (CCM) EMAC (e.g. Jöckel et al., 2016) was used for a multi-decadal hindcast reference simulation (RD1) driven by specified dynamics (SD), i.e. by observed meteorology, covering the period from 1980 – 2019. The RD1SD simulation was performed on the basis of specifications (i.e. boundary conditions) within the framework of CCMI2. The joint IGAC/SPARC CCM Initiative (CCMI) was established to coordinate IGAC and SPARC CCM evaluation and associated modeling activities. In the second phase of CCMI (i.e. CCMI2) the boundary conditions were adjusted regarding the recent IPCC climate assessment report (AR6, IPCC, 2021) and WMO scientific assessment of ozone (WMO, 2022).

With the CCM EMAC the RD1SD simulation was conducted in a T42 (triangular) spectral resolution of the ECHAM5 base model, corresponding to a quadratic Gaussian grid of 2.8° × 2.8° in latitude and longitude. The vertical resolution is with 90 (L90MA) model levels reaching up to 0.01 hPa into the middle atmosphere (MA; approximately 80 km). The RD1SD simulation has been branched off from restart files (i.e. 1 January 1979) of the corresponding free-running hindcast simulations and “nudged” by Newtonian relaxation towards ERA-5 reanalysis data (Hersbach et al., 2019). The Newtonian relaxation (nudging) of the ECHAM5 base model is applied in spectral space for the prognostic variables divergence, vorticity, temperature, and the (logarithm of the) surface pressure. The nudging strengths are not applied homogeneously in the vertical: the boundary layer and the stratosphere–middle atmosphere above 10 hPa are not nudged with transition layers of intermediate strengths in between. The nudging further implies that the sea surface temperatures (SSTs) and the sea-ice concentrations (SICs).

With respect to the CCM EMAC simulation results, we are determining the TCO3 by integrating the tropospheric ozone content from the surface up to heights with an ozone mixing ratio of 150 ppbv. This ozone mixing ratio is taken as the threshold value for recognizing the so-called ozonopause, which marks the region of strong vertical ozone gradient between the troposphere (with ozone mixing ratios of less than 150 ppbv) and stratosphere (with ozone mixing ratios of greater than 150 ppbv), independent of the analyzed geographical region (tropics, mid-latitudes, polar regions). Studies, which are based on the CCM EMAC RD1SD simulation data show that if one compares the determined

TCO3 values by using different definitions of the tropopause (e.g. using a fixed pressure layer or the temperature lapse rate criteria, i.e. the lowest level at which the lapse rate decreases to 2 K/km or less) or the ozonopause, the absolute TCO3 values usually differ by significantly lower than 10% and the distribution pattern hardly differ (Figure 1, top row). Using an ozonopause definition with a fixed ozone mixing ratio has the advantage of a smoother transition from the tropical region to the middle latitudes is guaranteed. Comparisons of the TCO3 global trend estimates using different definitions of the top of the troposphere indicate that the derived TCO3 trend pattern and values are looking very similar (Figure 1, bottom row).

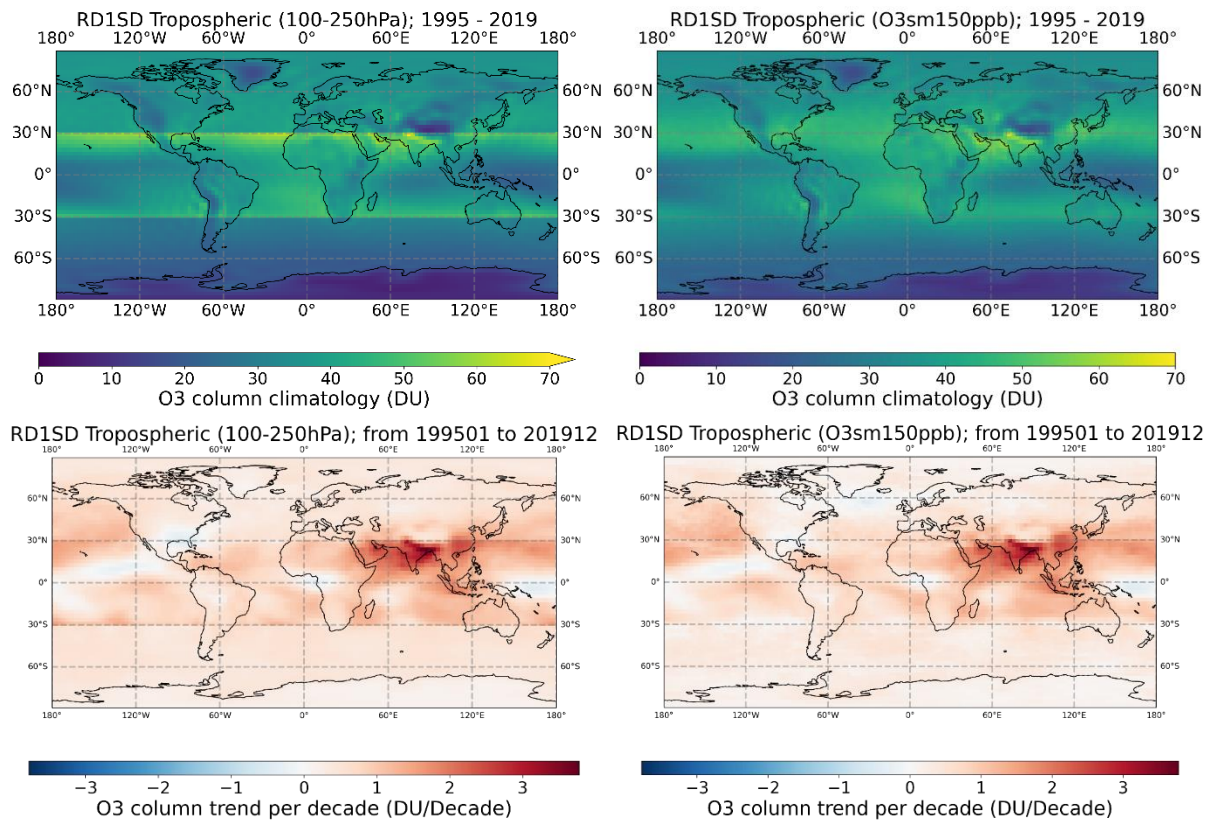


**Figure 1:** TCO3 climatological means (top row; in Dobson Unit, DU) and global TCO3 trends (bottom row; in DU per decade) derived from the CCM EMAC RD1SD simulation for the period 1995 – 2019 using different definitions with respect to the top of the troposphere: (left column) the pressure thresholds in the tropics (30°N – 30°S) is set on 100 hPa and in the extra-tropics (30° – 90°N/S) it is set on 250 hPa; (right column) the ozonopause is fixed to a mixing ratio of 150 ppbv for all latitudes.

### 3. TCO3 climatological means

In the paper by Gaudel et al. (2018) different tropospheric ozone climatologies are presented and discussed, showing annual mean distributions of TCO3 (in Dobson Unit, DU; Figure 2). One map (Figure 2, top left) is based on ozonesonde measurements (i.e. TOST, stands for Trajectory-mapped Ozonesonde dataset for the Stratosphere and Troposphere). TOST is a 3-dimensional, long-term ozone dataset derived from ozone soundings using a trajectory-based ozone mapping methodology. The other five maps are showing also TCO3 climatologies, which are derived from three satellite instrument measurements using different measurement techniques, i.e. OMI, MLS, and IASI. The results presented in Figure 2 has also been prepared applying various retrieval methods, which results in different sensitivities to ozone in the different parts of the troposphere and the therefore lead to different TCO3s value. Please note that the shown TOST product represents the geographic area from 80°N – 80°S and is considering the years from 2008 to 2012. The five space-based data sets are representing TCO3 for the period from 2010 to 2014 and the illustrations shown are limited to the latitudinal range from 60°N – 60°S.

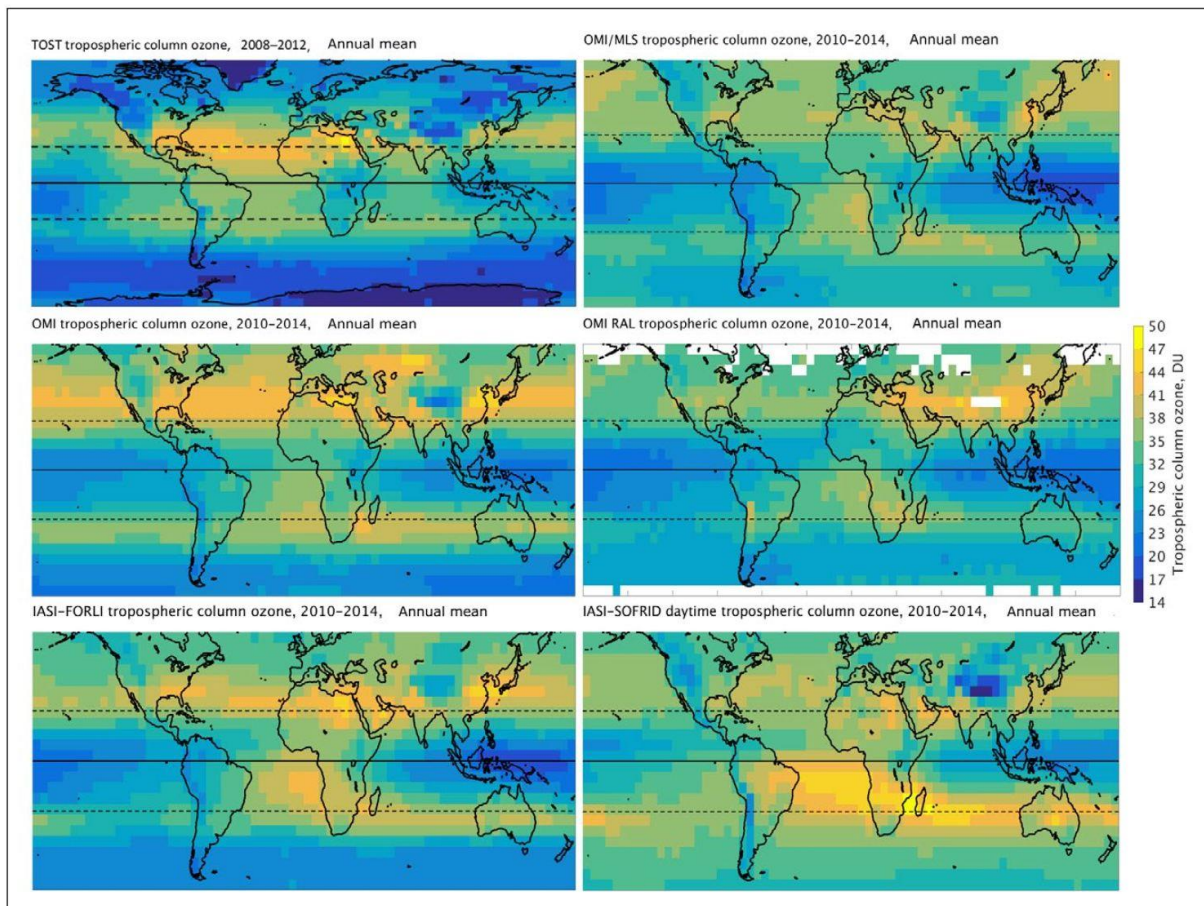


**Figure 10: Maps of annual mean TCO (DU) from five satellite products and ozonesondes (TOST).** Annual mean tropospheric column ozone (TCO) in Dobson unit (DU) as measured by TOST (top left), OMI/MLS (top right), OMI-SAO (middle left), OMI-RAL (middle right), IASI-FORLI (bottom left) and IASI-SOFRID (bottom right). The data are averaged over the period January 2010 through December 2014 and reported at 5° × 5° horizontal resolution, except for TOST, which covers the period 2008–2012. DOI: <https://doi.org/10.1525/elementa.291.f10>

**Figure 2:** This is Figure 10 (incl. the original caption) taken over from Gaudel et al. (2018), which is part of the TOAR.

There are obvious differences in the presented TCO3 distributions, not only in terms of the spatial patterns, but also in terms of the maximum and minimum column values. For instance, the different climatologies do not agree in mid- and higher latitudes. This is an indication for difficulties in generating robust TCO3 results at higher latitudes based on observations. Nonetheless, there are a few matches which can be identified, for instance low TCO3 values (around or below about 20 DU) can be found in the tropical region of Indonesia and the Pacific, high TCO3 values (around or higher than 40 DU) can be seen in the subtropical regions (20° – 30°N/S), or a pronounced TCO3 horizontal gradient over the North American continent with high TCO3 values in the eastern part and reduced TCO3 values in the western part associated with the Rocky Mountains. This indicates that a reliable derivation of the TCO3 is possible in the (sub-) tropics and mid-latitudes, independent of the used data set and the applied method for retrieving ozone.

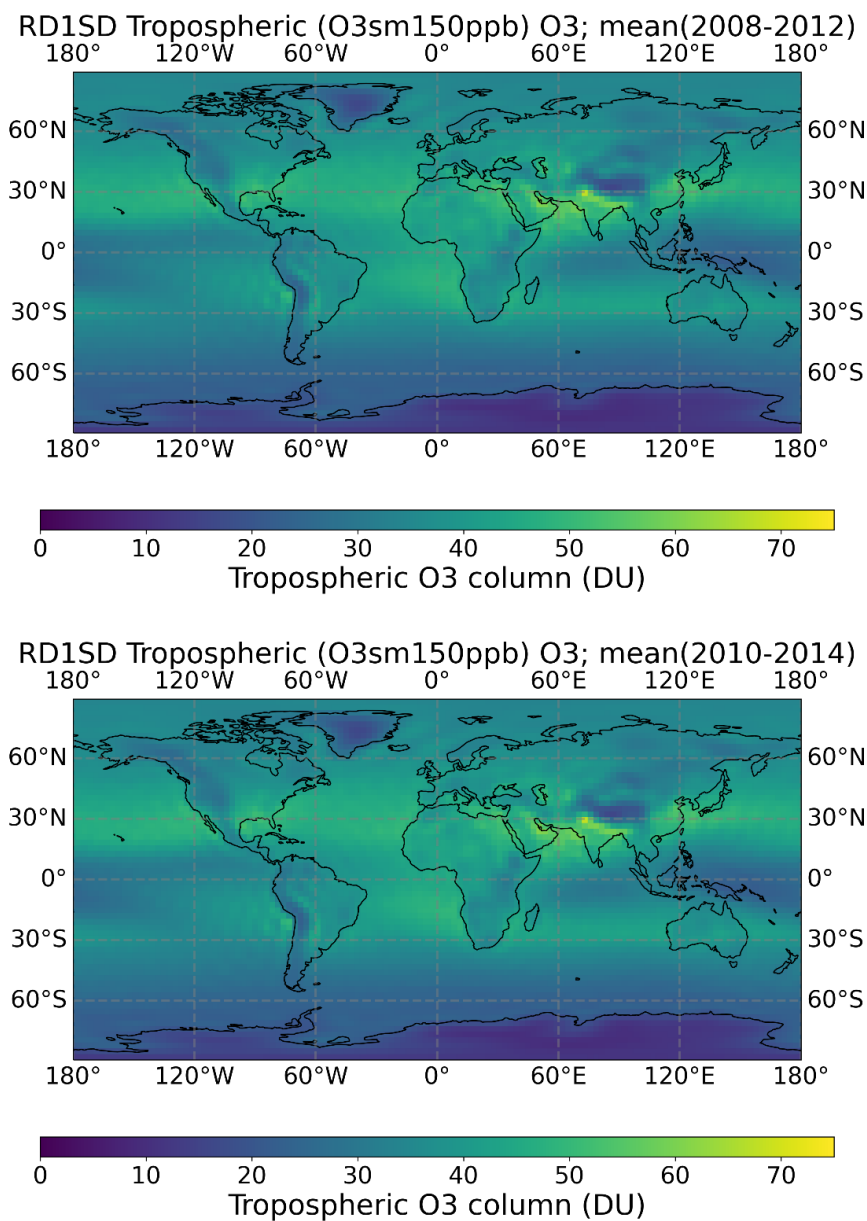


**Figure 3:** TCO3 global climatological annual means, which cover the periods 2008 – 2012 (top) and 2010 – 2014 (bottom) as derived from the CCM EMAC RD1SD simulation. The ozonopause is fixed to a mixing ratio of 150 ppbv for all latitudes.

The annual mean global TCO<sub>3</sub> distribution (from 90°N – 90°S) for the 5-year means of 2008 – 2012 and 2010 – 2014 as derived from the CCM EMAC RD1SD simulation (Figure 3) show in parts a consistent result in comparison with the presented climatologies based on observations (Figure 2). The tropical region (in particular over Indonesia and the Pacific) indicate low TCO<sub>3</sub> values, whereas the subtropical regions (north and south) are showing maximum TCO<sub>3</sub> values (around or higher than 50 DU), which are higher than those derived from observations. The TCO<sub>3</sub> East-West gradient over North America is also identified in the model data. The model result indicates plausible low TCO<sub>3</sub> values in both polar regions, especially very low TCO<sub>3</sub> values (around 10 DU) are seen in the Antarctic region.

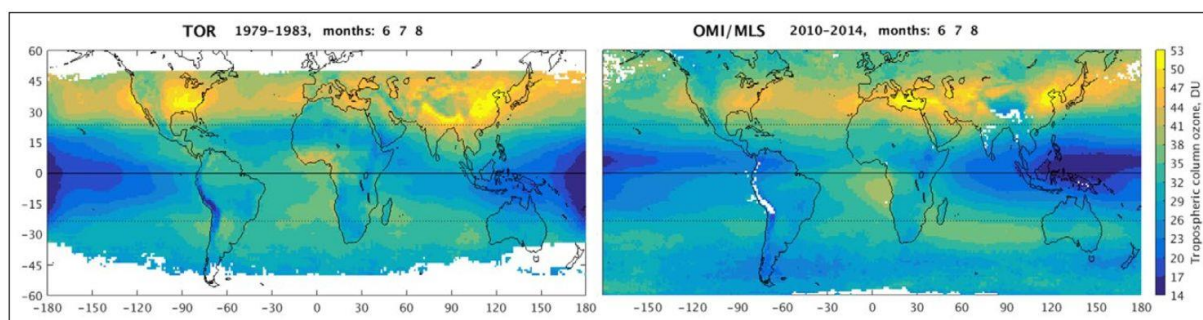


**Figure 22: June–July–August mean TCO (DU) measured by TOR and OMI/MLS.** June–July–August tropospheric column ozone (TCO) in Dobson unit (DU) as measured by the TOR product for 1979–1983 (left) and OMI/MLS for 2010–2014 (right). DOI: <https://doi.org/10.1525/elementa.291.f22>

**Figure 4:** This is Figure 22 (incl. the original caption) taken over from Gaudel et al. (2018), which is part of the TOAR.

To discuss the seasonal dependency, TCO<sub>3</sub> climatological means for the months June, July, and August (JJA) are considered. In the left part of Figure 4, the results of Tropospheric Ozone Residual (TOR) representing the period from 1979 – 1983. TOR was the first satellite product to quantify tropospheric ozone, providing TCO<sub>3</sub> values in a horizontal resolution of 1° × 1.25° across much of the globe from 50°N – 50°N). For comparison, the corresponding OMI/MLS TCO<sub>3</sub> values representing the years from 2010 to 2014 are shown in the right part of Figure 4. The absolute TCO<sub>3</sub> values are different (as expected), but the detected TCO<sub>3</sub> distribution is similar, with lower TCO<sub>3</sub> in the tropical region (with lowest values over Indonesia and the Pacific), higher TCO<sub>3</sub> values in the northern (summer) subtropical region, and the mentioned TCO<sub>3</sub> East-West gradient over North America.

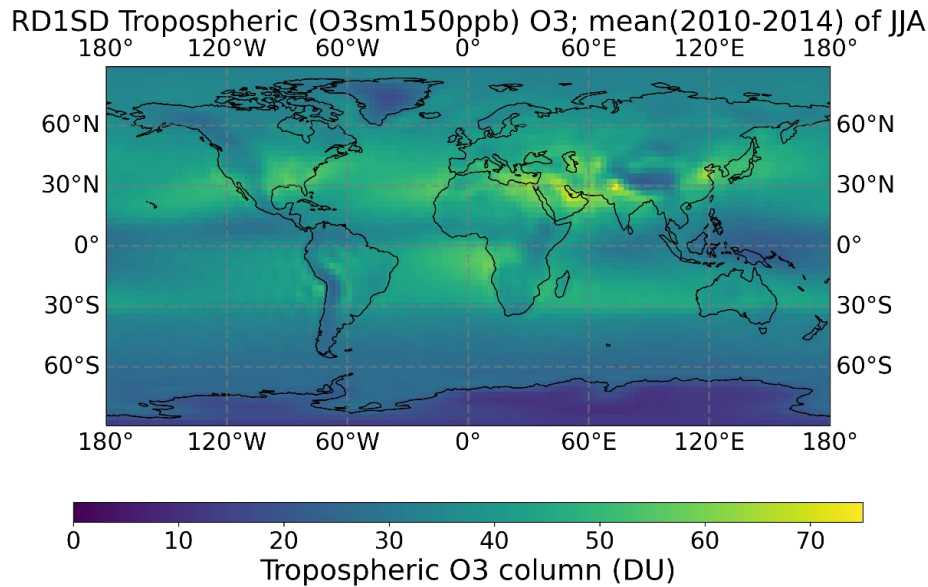


**Figure 5:** TCO3 global climatology for June, July, and August (JJA), which covers the period from 2010 – 2014, as derived from the RD1SD simulation. The ozonopause is fixed to a mixing ratio of 150 ppbv for all latitudes.

Again, the corresponding model result (here the JJA mean for 2010 – 2014) derived from the CCM EMAC simulation RD1SD shows very similar results, with low TCO3 values in the tropics (most pronounced over Indonesia), higher TCO3 values in the northern subtropics, and again the clear TCO3 East-West gradient over North America (Figure 5). The differences between the northern and southern subtropical region are not as pronounced as indicated in the TCO3 values derived from observations. Overall, the TCO3 distribution especially in the subtropical and mid-latitude regions are in very good agreement with the TCO3 OMI/MLS product.

In the following the climatological mean TCO3 derived from TTOC\_CCD (K.-P. Heue, DLR-IMF) for the period 1995 – 2022 are compared with the results derived from the CCM EMAC simulation RD1SD (for 1995 – 2019). The ozone data product TTOC\_CCD consider the total column from the surface up to 200 hPa.

Figure 6 (upper part) is showing the TCO3 climatological mean (1995 – 2022) for the tropical region (20°S – 20°N) based on the TTOC\_CCD data. The pronounced ozone minimum identified in the Pacific region and an obvious maximum in the southern tropical Atlantic is the well-known wave-one structure first discussed by Thompson et al. (2003). The corresponding CCM EMAC RD1SD (Figure 6, middle part) simulation results show the same tropical pattern, but the difference between the maximum and minimum TCO3 values in the tropical region is significantly lower (i.e. about 40 DU in TTOC\_CCD as opposed to about 30 DU in RD1SD). For comparison, the entire TCO3 (using the threshold value of 150 ppbv ozone mixing ratio instead of the fixed pressure level 200 hPa) are showing similar results but in general the TCO3 values are (as expected) slightly enhanced (Figure 6, lower part). In summary, it can be said that the tropical TCO3 values and the distribution from TTOC\_CCD agree relatively well with the corresponding results from the CCM EMAC RD1SD.

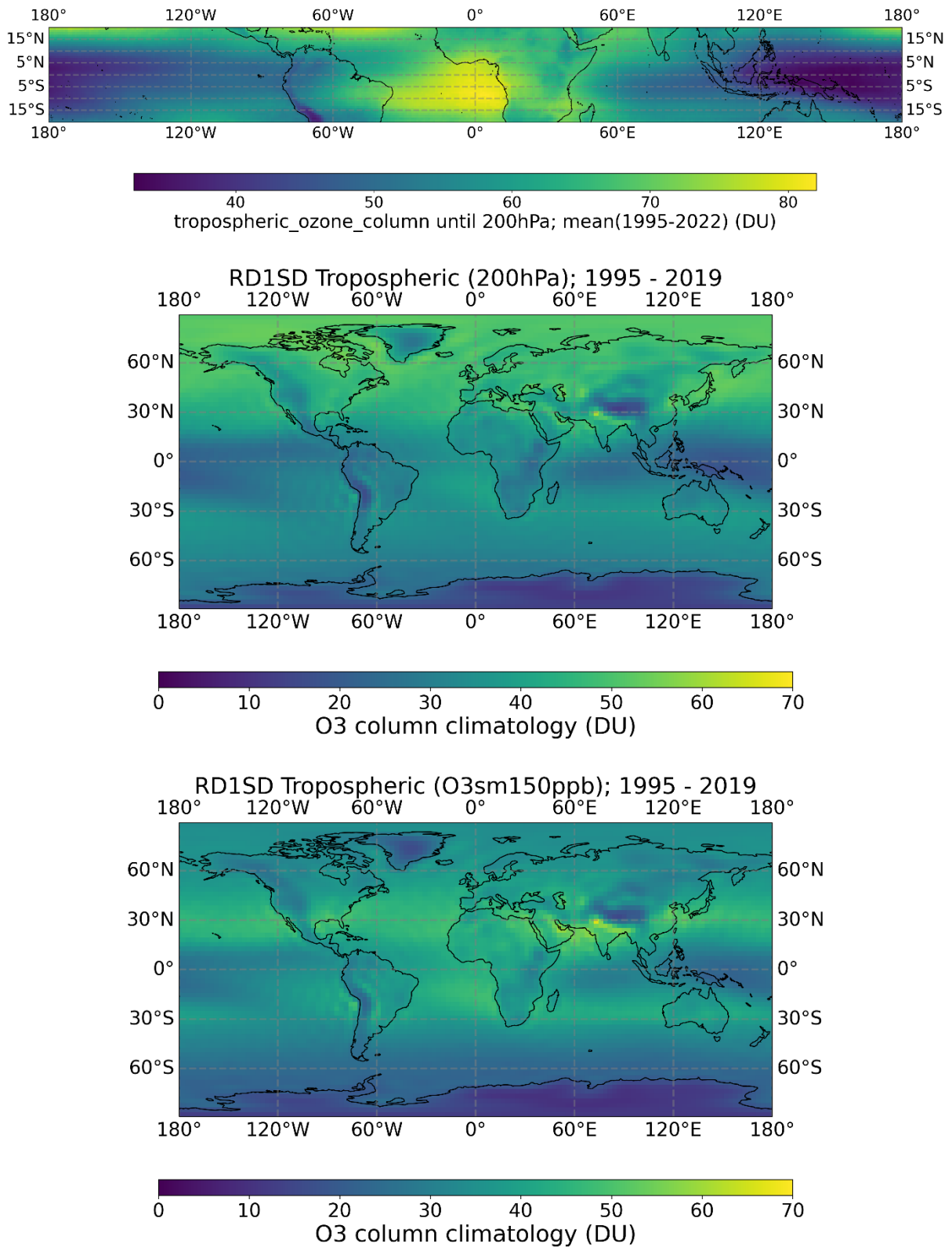
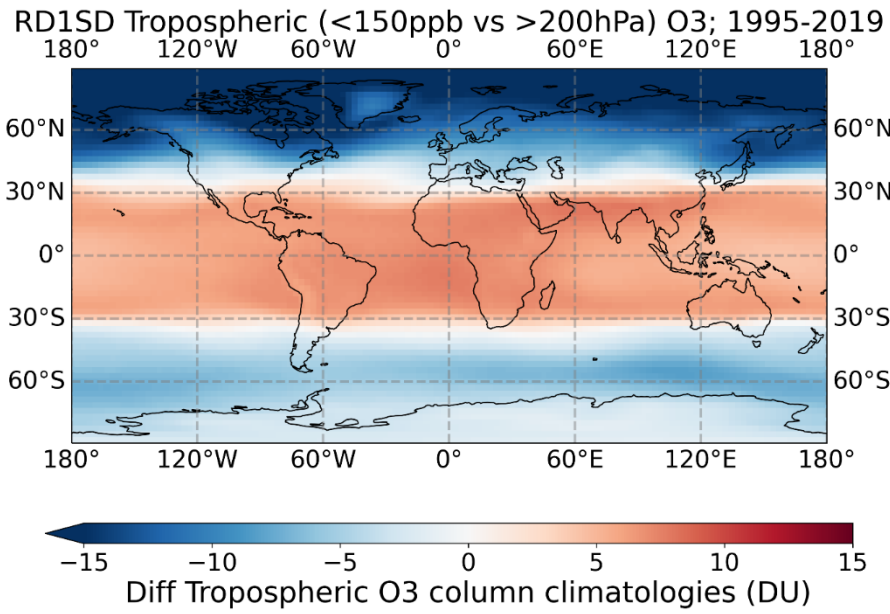


**Figure 6:** (Top) Climatological mean TCO3 derived from TTOC\_CCD (1995 – 2022). The tropical tropospheric ozone column is determined globally from the surface up to 200 hPa. (Middle) For comparison, the global distribution of TCO3 values from the RD1SD simulation is also calculated from the surface up to 200 hPa. (Bottom) In addition, the TCO3 from the CCM EMAC RD1SD simulation using the ozone threshold mixing ratio of 150 ppbv, describing the so-called ozonopause, is shown. Please note the different color scales.



**Supplement to Figure 6:** Difference of the TCO<sub>3</sub> derived from the CCM EMAC RD1SD simulation considering the different definitions of the tropospheric ozone columns, i.e. using the ozone threshold mixing ratio of 150 ppbv versus the 200 hPa pressure level. The delta TCO<sub>3</sub> values in the tropical region are below about 7 DU, which is in the order of less than 10%.

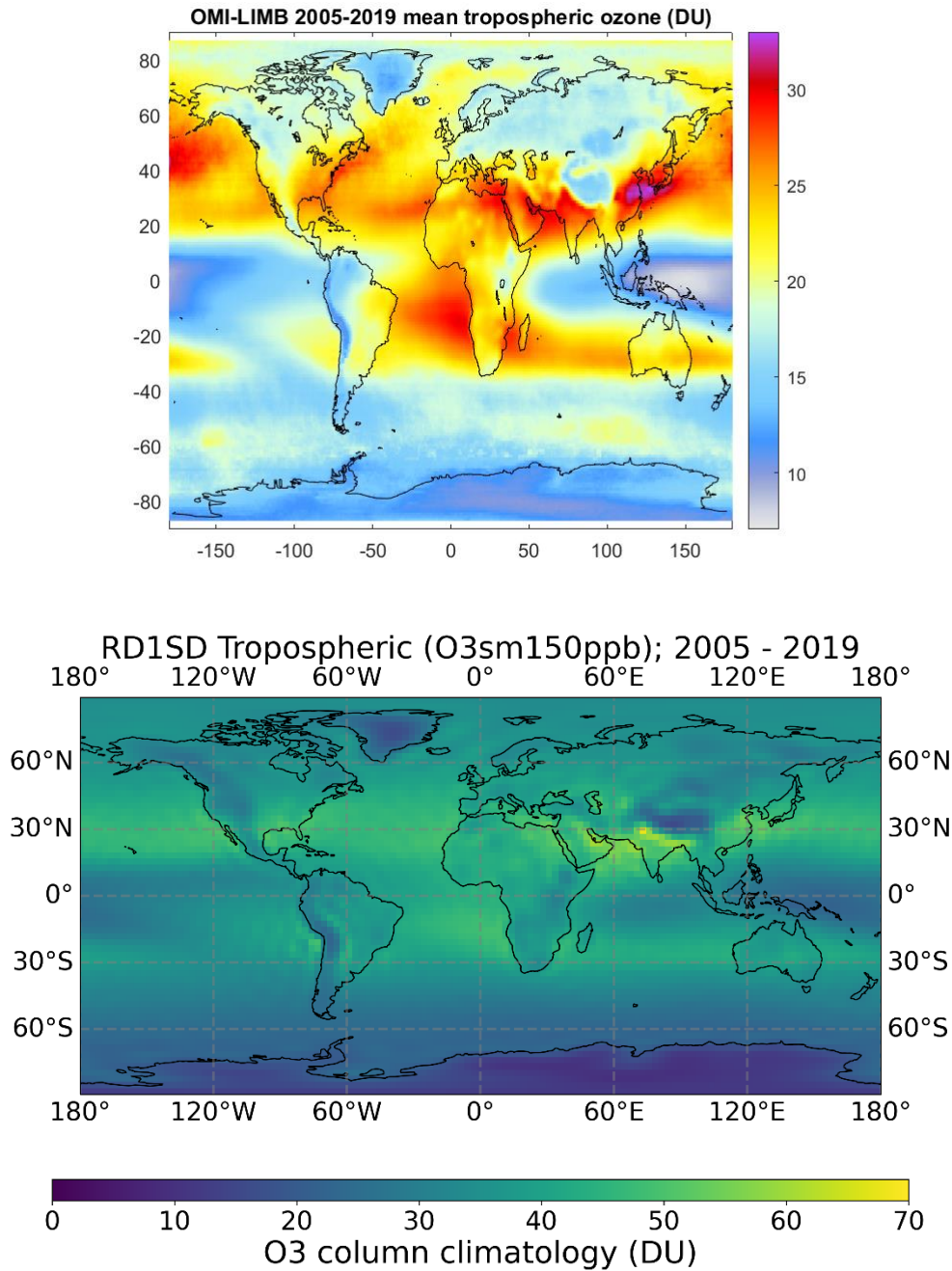


**Figure 7:** (Top) The SUNLIT-OMI-LIMB tropospheric ozone column (TCO3) climatology computed for the years 2005-2019. (Bottom) The corresponding TCO3 climatological mean as derived from the CCM EMAC RD1SD simulation. Please note: The TCO3 values for OMI-LIMB are calculated from the surface up to 3 km below the tropopause, whereas the modelled TCO3 is considering the complete troposphere up to the ozonopause, which is determined by using the ozone mixing ratio threshold fixed to 150 ppbv for all latitudes.

In the following the climatological mean TCO3 derived from SUNLIT-OMI-LIMB (V. Sofieva, FMI) for the period 2005 – 2019 are compared with the results derived from the CCM EMAC simulation RD1SD (for 2005 – 2019). The ozone data product OMI-LIMB consider the total column from the surface up to 3 km below the tropopause.

The TCO<sub>3</sub> climatologies presented Figure 7, which are derived from SUNLIT-OMI-LIMB and the CCM EMAC RD1SD simulation, show a very good agreement regarding the distribution patterns, i.e. the regions with high and low TCO<sub>3</sub> values are very well represented. For instance, high TCO<sub>3</sub> values are determined in the subtropical regions, and much lower values are found in the tropics, mostly pronounced over Indonesia. Very low TCO<sub>3</sub> values over Antarctica are identified in both data sets. A nice agreement is also found for the northern polar (Arctic) region with strikingly low TCO<sub>3</sub> values over Greenland in both data sets. Furthermore, it can also be seen here that the east-west gradient over North America is well represented in the climatological means of TCO<sub>3</sub> from OMI-LIMB and RD1SD TCO<sub>3</sub> data. It must be noted that there are sometimes larger differences with regard to the absolute TCO<sub>3</sub> values, for instance in the south-east Asian region.

#### 4. TCO3 trends

- TCO3 trends discussed in recent publications (peer-reviewed journals); comparison with climate model results

We start with the trend analyses presented in TOAR (Gaudel et al., 2018). The data records are the same as those in Section 3. Please note that the presented trend analyzes in Figure 8 are based on slightly different time periods and the length of the time series is also different (9-12 years). It is immediately noticeable that the derived trends differ greatly, even in their sign. The greatest agreement in terms of positive trends is identified in the tropical region (20°N – 20°S). Other matches are hard to identify.

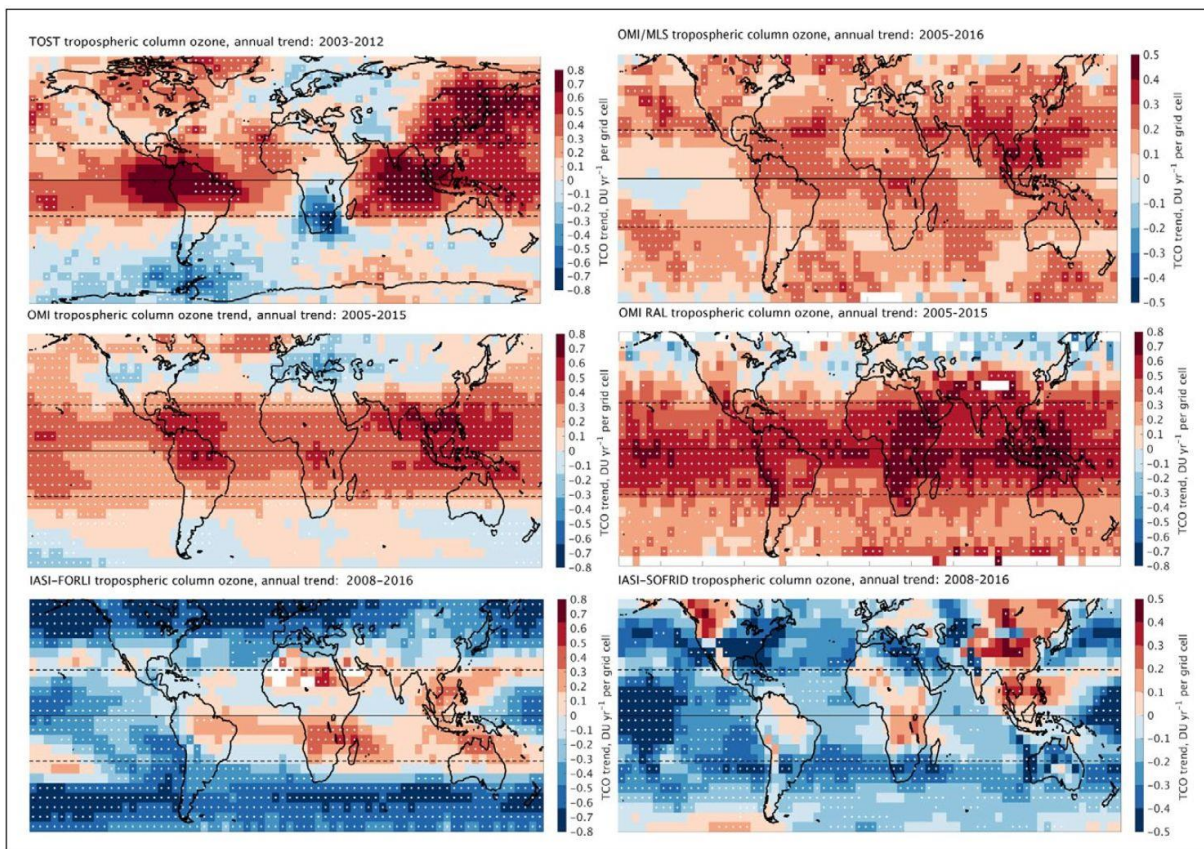


**Figure 24: Maps of trends of TCO (DU yr<sup>-1</sup>) from five satellite products and ozonesondes (TOST).** (top left) 2003–2012 TOST ozonesonde annual tropospheric column ozone (TCO) trends in Dobson unit per year (DU yr<sup>-1</sup>) for each 5° × 5° grid cell between 80°S–80°N. White dots indicate grid cells with statistically significant trends. Also shown are satellite products between 60°S–60°N: (top right) OMI/MLS, 2005–2016, (middle left) OMI-SAO, 2005–2016, (middle right) OMI-RAL, 2005–2015, (bottom left) IASI-FORLI, 2008–2016, and (bottom right) IASI-SOFRID, 2008–2015. Note that OMI/MLS and IASI-SOFRID have different color scales from the rest. Trends in this figure are based on least-squares linear regression and reported with 95% confidence intervals and p-values. DOI: <https://doi.org/10.1525/elementa.291.f24>

**Figure 8:** This is Figure 24 (incl. the original caption) taken over from Gaudel et al. (2018), which is part of the TOAR. Please note that the given trends are given in Dobson Unit (DU) per year.

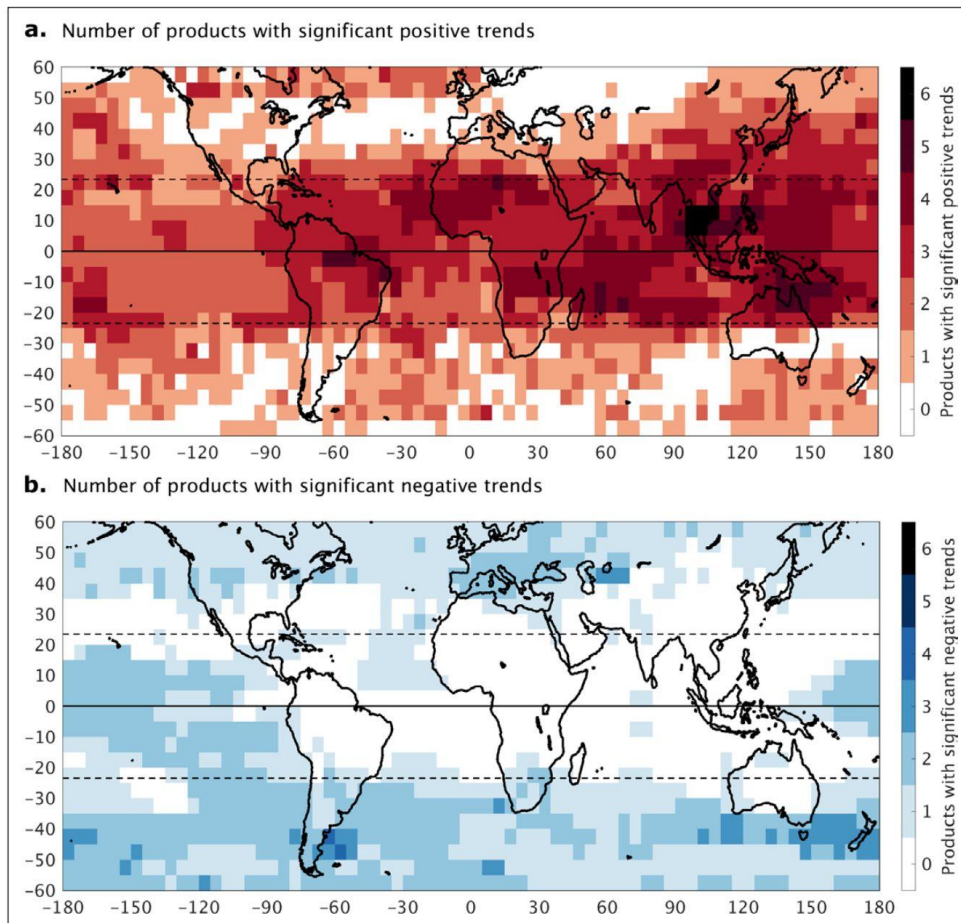


**Figure 25: Number of products from Figure 24 with statistically significant positive and negative trends per grid cell. (a)** Number of products from Figure 24 that indicate a statistically significant positive trend in each  $5^\circ \times 5^\circ$  grid cell. All six products shows significant ozone increases in five grid cells, all above Southeast Asia. **(b)** As in (a) but for statistically significant negative trends. DOI: <https://doi.org/10.1525/elementa.291.f25>

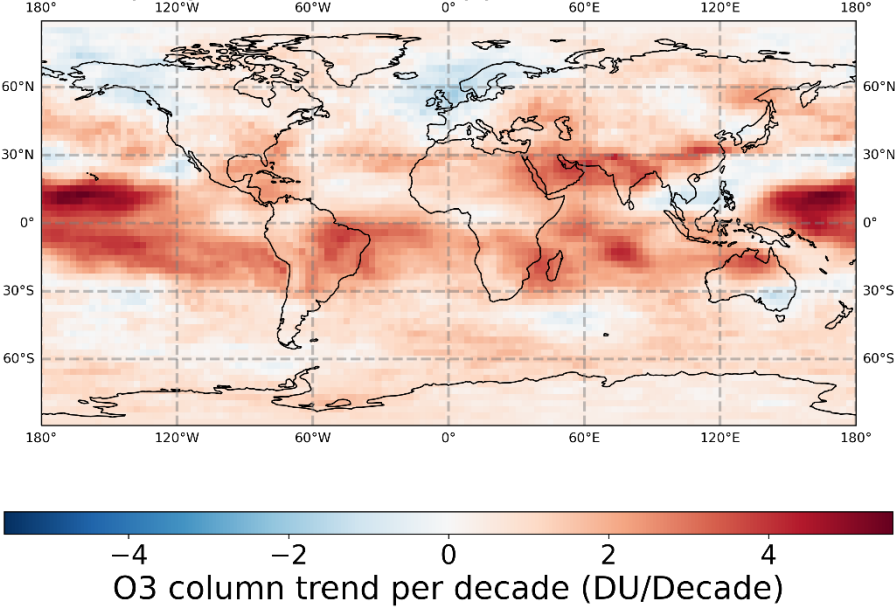
**Figure 9:** This is Figure 25 (incl. the original caption) taken over from Gaudel et al. (2018), which is part of the TOAR.

Figure 9 provides a simple but nice possibility to recognize other regions with robust tropospheric ozone trends. Outstanding regions with clear positive tropospheric ozone trend are detected in the region of Southeast Asia, equatorial Brazil, central northern Africa, the tropical South Indian Ocean and northern Australia. Southeast Asia is the most extensive region (Gaudel et al., 2018), which is also mostly in line with the decadal tropospheric ozone trends since 1994 as presented in IPCC (2021; see Figure 6.5 in Chapter 6).

For comparison, Figure 10 shows the corresponding TCO<sub>3</sub> trend analyses determined from the CCM EMAC RD1SD simulation. In both illustrations (i.e. from 2003 – 2012 and 2005 – 2014) the overall trend patterns look very similar, but the strengths of the trends differ significantly in some regions. Although the two periods analyzed hardly differ (shifted by only two years), there are some notable regional differences (e.g. South America, tropical Pacific). Nevertheless, clear positive trends can be also found in the CCM EMAC over the African continent (north and south of the equatorial region) and northern Australia, which are in line with the trends derived from the observational data sets. Obvious trends in southeast Asia are also evident in the CCM, but they are not quite as pronounced as observed. Overall one can summarize that some of the most noticeable TCO<sub>3</sub> positive trends

determined from the CCM EMAC RD1SD simulation agree with those from the observations discussed in TOAR.

RD1SD Tropospheric (O3sm150ppb); from 200301 to 201212



RD1SD Tropospheric (O3sm150ppb); from 200501 to 201412

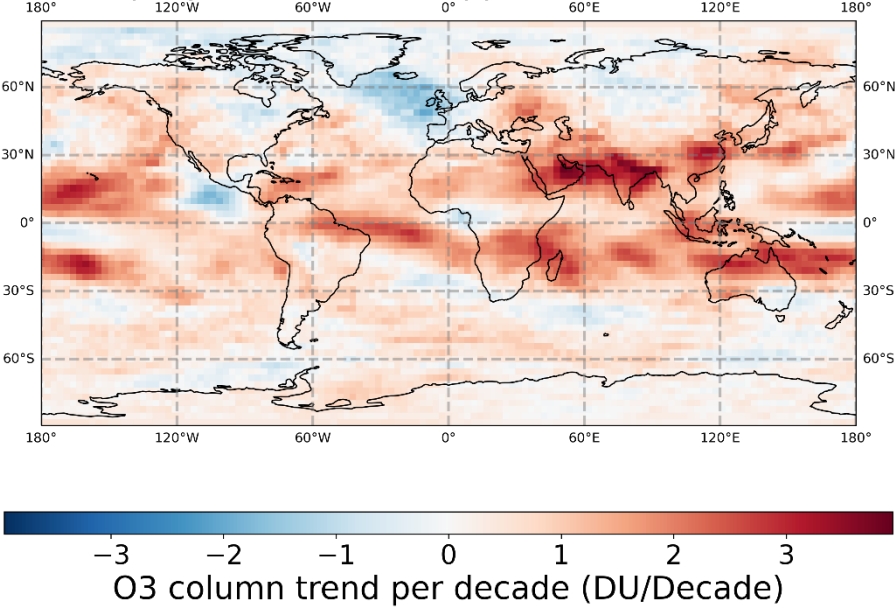


**Figure 10:** Trend analysis of TCO3 from the CCM EMAC RD1SD simulation for the period 2003 – 2012 (top) and 2005 – 2014 (bottom). Please note that the given trends are in Dobson Unit (DU) per decade and that the minimum/maximum values of the color scales are slightly different.

For completeness, in recent years additional studies with respect to tropospheric ozone trends have been published (e.g., Ziemke et al., 2019), some of them consider also trends analyses based on reanalysis data sets and other CCM studies (Fiore et al., 2022; Wang et al., 2022; Christiansen et al., 2022). They will be briefly discussed in the following.

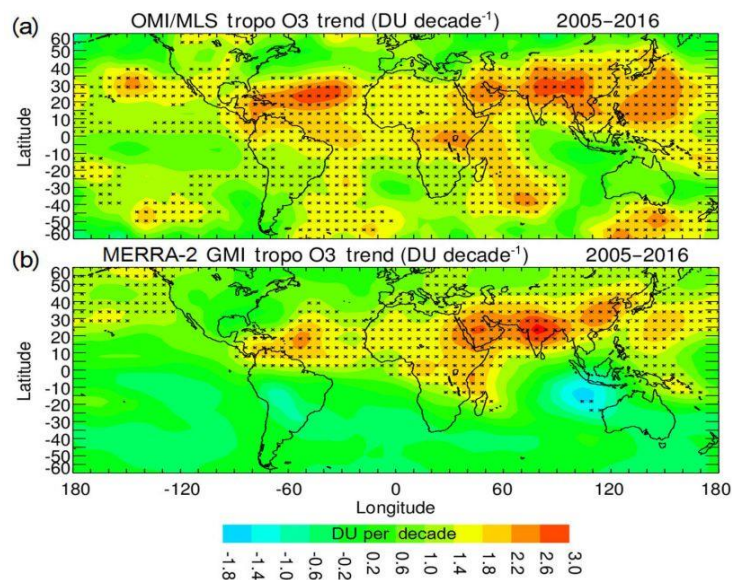


**Figure 1.** (a) Trends in OMI/MLS TCO (in  $\text{DU decade}^{-1}$ ) for 2005–2016. Asterisks denote grid points where trends are statistically significant at the  $2\sigma$  level. (b) Same as (a) except for MERRA-2 GMI TCO.

*Figure 11:* This is Figure 1 (incl. the original caption) taken over from Ziemke et al. (2019).

In the paper by Ziemke et al. (2019) TCO<sub>3</sub> data from OMI/MLS are compared with the TCO<sub>3</sub> values from MERRA-2 GMI (reanalysis) for the period from 2005 – 2016. Both trend images presented in Figure 11 are indicating the strongest trends in the (sub-)tropical region, but they differ significantly from one another showing different change pattern and trend values. The formerly discussed regions with robust positive TCO<sub>3</sub> trends, i.e. equatorial Brazil, the African continent, northern Australia, and southeast Asia, are not visible in the same way (cp. Figures 8 and 10).

In Ziemke et al. (2019) the trend analysis has been extended for the tropical region ( $25^{\circ}\text{N} - 25^{\circ}\text{S}$ ), studying first the period from 1979 to 2005 (Figure 12), comparing the results based on TOMs and MERRA-2 GMI. Again, obvious differences can be found in the trend analyses. The authors stated: “As with OMI/MLS and GMI TCO trends in Fig. 1 there are discrepancies between the TOMS and model TCO trends in Fig. 4. For TOMS TCO in Fig. 4 there are regions of negative trends (in blue) of as much as  $-0.6 \text{ DU decade}^{-1}$  over ocean in both hemispheres that are not explainable.” (Ziemke et al., 2019). The merged ozone data record (i.e. TOMS / OMI/MLS, spanning 1979 – 2016) has been compared with the respective MERRA-2 GMI TCO<sub>3</sub> record, allowing the determinations of the trends for this much longer period in the tropics (Figure 12). In this case, the trend statements are very similar regarding the change pattern and trend values, with the largest positive trend in southeast Asia.

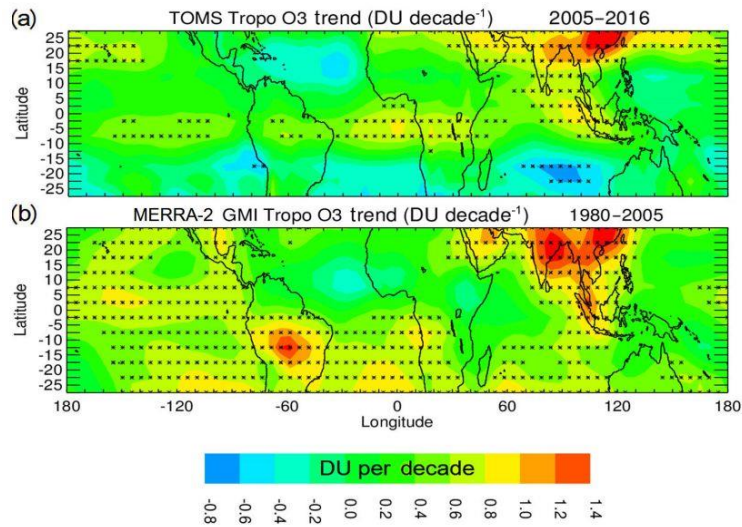


**Figure 4.** (a) Trends ( $\text{DU decade}^{-1}$ ) calculated for TOMS CCD TCO measurements for the years 1979–2005. Asterisks denote grid points where trends are statistically significant at the  $2\sigma$  level. (b) Similar to (a), but for MERRA-2 GMI TCO and for 1980–2005.

**Figure 12:** This is Figure 4 (incl. the original caption) taken over from Ziemke et al. (2019). Please note the error in the head line of upper part of the figure: it must be 1979 – 2005 (instead of 2005 – 2016).

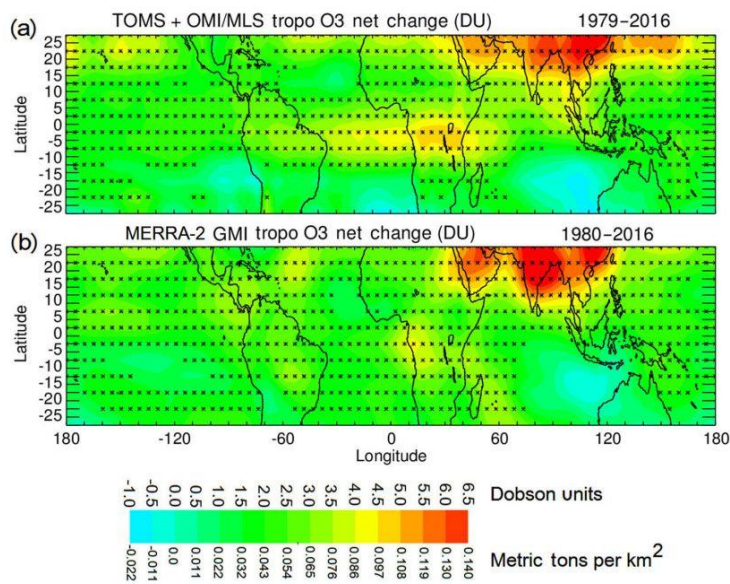
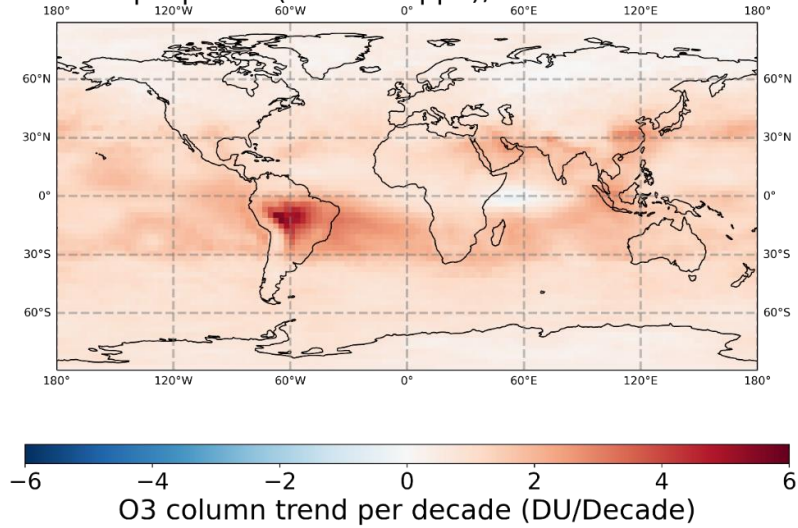


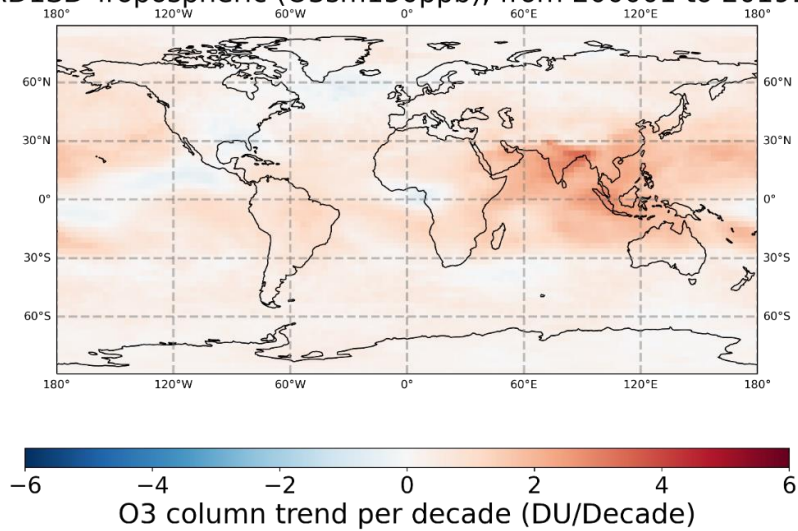
**Figure 7.** (a) Net changes in TOMS and OMI/MLS TCO calculated for their combined time records (1979–2016). The net changes for TCO are shown in the color bar in both DU and metric tons of ozone per  $\text{km}^2$  ( $1 \text{ DU} \equiv 0.0214 \text{ t km}^{-2}$  for ozone). Asterisks denote grid points where net changes are statistically significant at the  $2\sigma$  noise level. (b) Similar to (a), but for GMI TCO and years 1980–2016. Net change for GMI TCO is determined similar to the satellite measurements by adding together the net changes for the two records (i.e., for GMI, the 1980–2005 and 2005–2016 periods).

**Figure 13:** This is Figure 7 (incl. the original caption) taken over from Ziemke et al. (2019).

RD1SD Tropospheric (O3sm150ppb); from 198001 to 199912



RD1SD Tropospheric (O3sm150ppb); from 200001 to 201912



RD1SD Tropospheric (O3sm150ppb); from 198001 to 201912

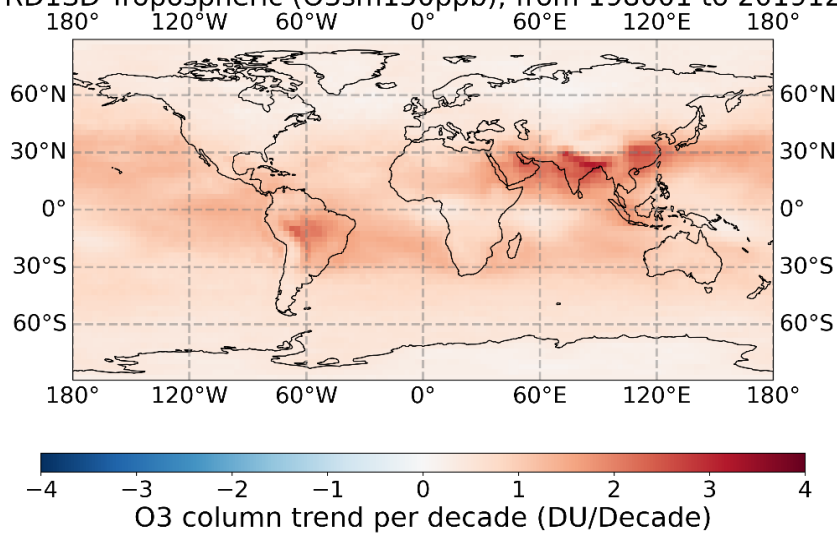


**Figure 14:** Long-term trend analyses based on the results derived from the CCM EMAC RD1SD simulation: Top: 1980 – 1999, Middle: 2000 – 2019, Bottom: 1980 – 2019. Please note the different color scales (different minimum/maximum values).

Figure 14 (lower part, 1980 - 2019) shows agreement with results presented in Figure 13 (1979/1980 – 2016) for the (sub-)tropical region ( $25^{\circ}$  N –  $25^{\circ}$  S), indicating strongest positive trends over the Indian continent and Indonesia. Some agreement can be also seen over South America and the southern part of the African continent with obvious positive ozone trends. The stronger trends detected in the CCM EMAC RD1SD simulation over Central South America are caused in the first half of the period analyzed (i.e. 1980 – 1999, see Figure 14, upper part). This finding is in line with respective results identified in the MERRA-2 GMI data (see Figure 12, lower part). As can be seen for Figure 14 (middle part), for the period 2000 – 2019 the RD1SD data the TCO3 trend over South America is clearly weakening (in line with the results presented in Figure 11, which based on OMI/MLS and MERRA-2 GMI). The RD1SD data for this time period (2000 – 2019) is showing enhanced ozone trends over India and Indonesia in comparison with the time period of 1980 – 1999.

- TCO3 trends derived from ESA Ozone\_cci data products

In the following, firstly we are looking at the derived TCO3 trends based on the SUNLIT-OMI-LIMB data and the CCM EMAC RD1SD simulation (Figure 15). First of all, it can be noted that the calculated trends are of the same order of magnitude, i.e.  $\pm 3$ -4 DU/decade. Focusing on the linear trend estimates (top right and bottom) it is obvious that the trend pattern is looking partly different, although some matches can be identified. The trend estimates agree in particular over North and Middle America (including the neighboring East Pacific and West Atlantic regions), in the Amazon region, or India and South-East Asia. Differences become apparent over the Indian Ocean and further east to Australia. Positive TOC3 trends are identified in the latitude region of  $30^\circ - 60^\circ\text{S}$  in both data sets. The OMI-LIMB and the RD1SD data differ at higher latitudes in both hemispheres. More analyses on this point can be found in Chapter 5.

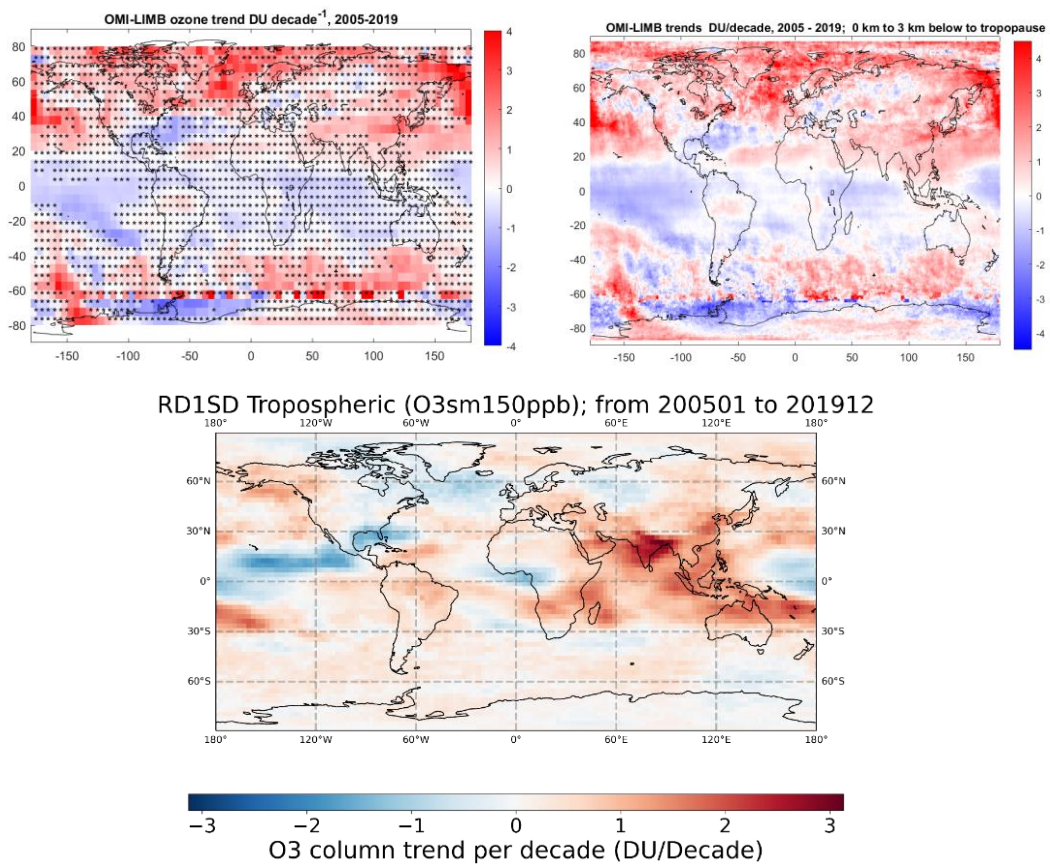


**Figure 15:** (Top left) SUNLIT-OMI -LIMB tropospheric ozone column (from ground to 3 km below the tropopause) trends in DU/decade. Trends are estimated using multiple linear regression applied to deseasonalized anomalies. Solar cycle, QBO and ENSO are included as proxies. The resolution of the map is 5x5 deg. Stars indicate the regions where the estimated trends are not statistically significant. (Top right) OMI-LIMB tropospheric ozone trends using the data from years 2005 – 2019. The trends are estimated as linear fit of yearly data. The resolution of the map is 1x1 deg. (Bottom) Respective linear trend estimate based on the CCM EMAC RD1SD simulation.

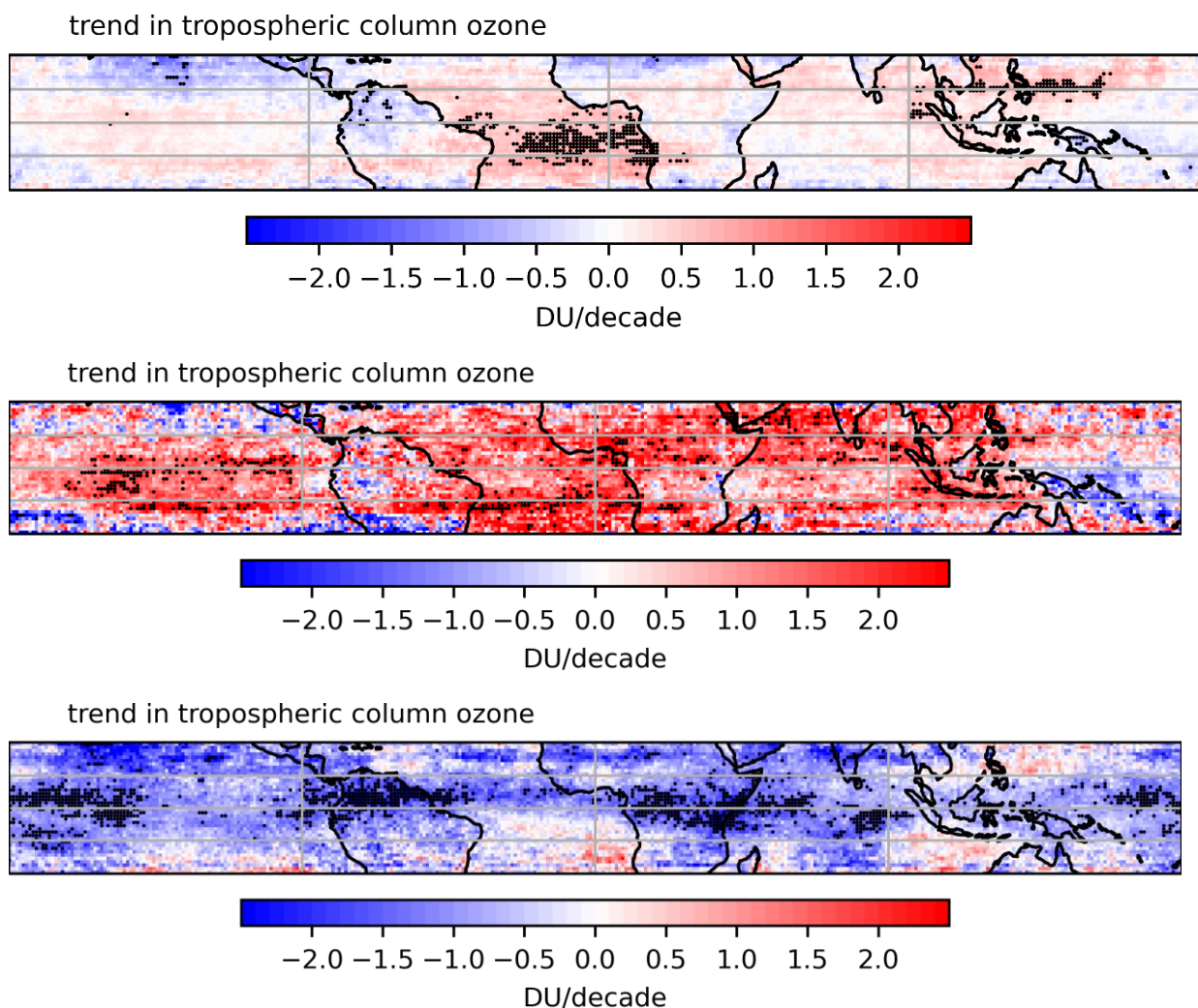


**Figure 16:** Analyses based on the TTOC\_CCD data. Top: 1995 – 2022 (status in 02-2023); Middle: 1995 – 2008 (07-2023); Bottom: 2008-2022 (status in 07-2023). Tropical Tropospheric Ozone Column trends (20°S – 20°N) evaluated using TTOC\_CCD. Stars indicate the regions, where the trends are statistically significant at 95% confidence level.

Now we are focusing on the TTOC\_CCD (Convective Cloud Differential data) climate product. The tropical tropospheric column ozone (TTCO3) has been retrieved with the convective cloud differential (CCD) method. It covers the tropical belt from 20°N – 20°S in the years from 1995 – 2022, i.e. GOME, SCIAMACHY, OMI, GOME-2 (A,B and C) and TROPOMI (monthly averages on a  $1^\circ \times 1^\circ$  (latitude  $\times$  longitude); latest updates relative to Heue et al. (2016). In Figure 16 the corresponding trend analyses are presented covering the periods 1995 – 2022 (upper part), 1995 – 2007 (middle part), and 2008 – 2022 (lower part). The two analyzed sub-periods obviously differ significantly in terms of their sign of trend. In the first time period in most tropical areas the trend of the TTCO3 is positive whereas it is mostly negative in the second period. The long-term trend estimated for the complete period (i.e. 1995 – 2022) are mostly relative weak in the order of about  $\pm 1$  DU/decade.

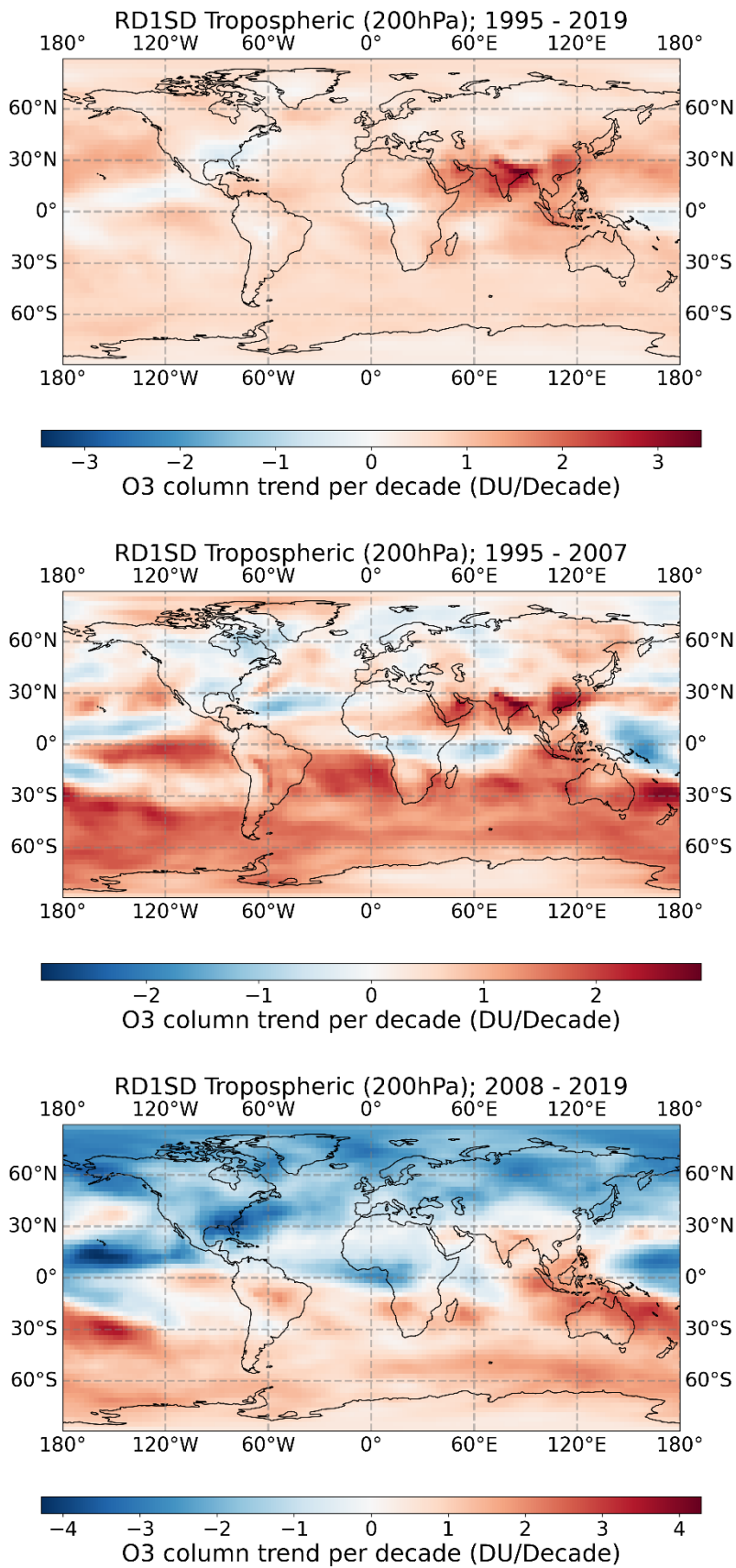


**Figure 17:** Analyses based on the results of the CCM EMAC RD1SD simulation. Attention: Different color scales!

Figure 17 shows the corresponding TCO<sub>3</sub> trend results as derived from the CCM EMAC RD1SD simulation. Focusing on the tropics, the long-term trend estimated for the complete period (i.e. 1995 – 2019) looks similar to T<sub>TOC\_CCD</sub> regarding the overall trend pattern over the tropical oceans (i.e. Pacific, Atlantic and Indian ocean) and also in parts over the adjacent continents (i.e. South America and Africa; Figure 17, top part). The T<sub>TCO<sub>3</sub></sub> trends determined for the two sub-periods from the CCM EMAC RD1SD simulation results (Figure 17, middle and lower part) show good agreement with the T<sub>TOC\_CCD</sub> results (Figure 16, middle and lower part), again in particular over the oceans. In addition, for the period 1995 – 2007 (middle parts in Figures 16 and 17) there are some nice matches over Brazil, South India and Indonesia. For the period 2008 – 2019 (lower parts of Figures 16 and 17) there is a match over Africa, but over South America, South India and Indonesia they do not agree, i.e. the signs of trends are opposite.

The model results presented in Figure 17 provide some additional information how the TCO<sub>3</sub> trends derived for the tropics are embedded into the global picture. Interestingly, the extra-tropical regions behave very differently.

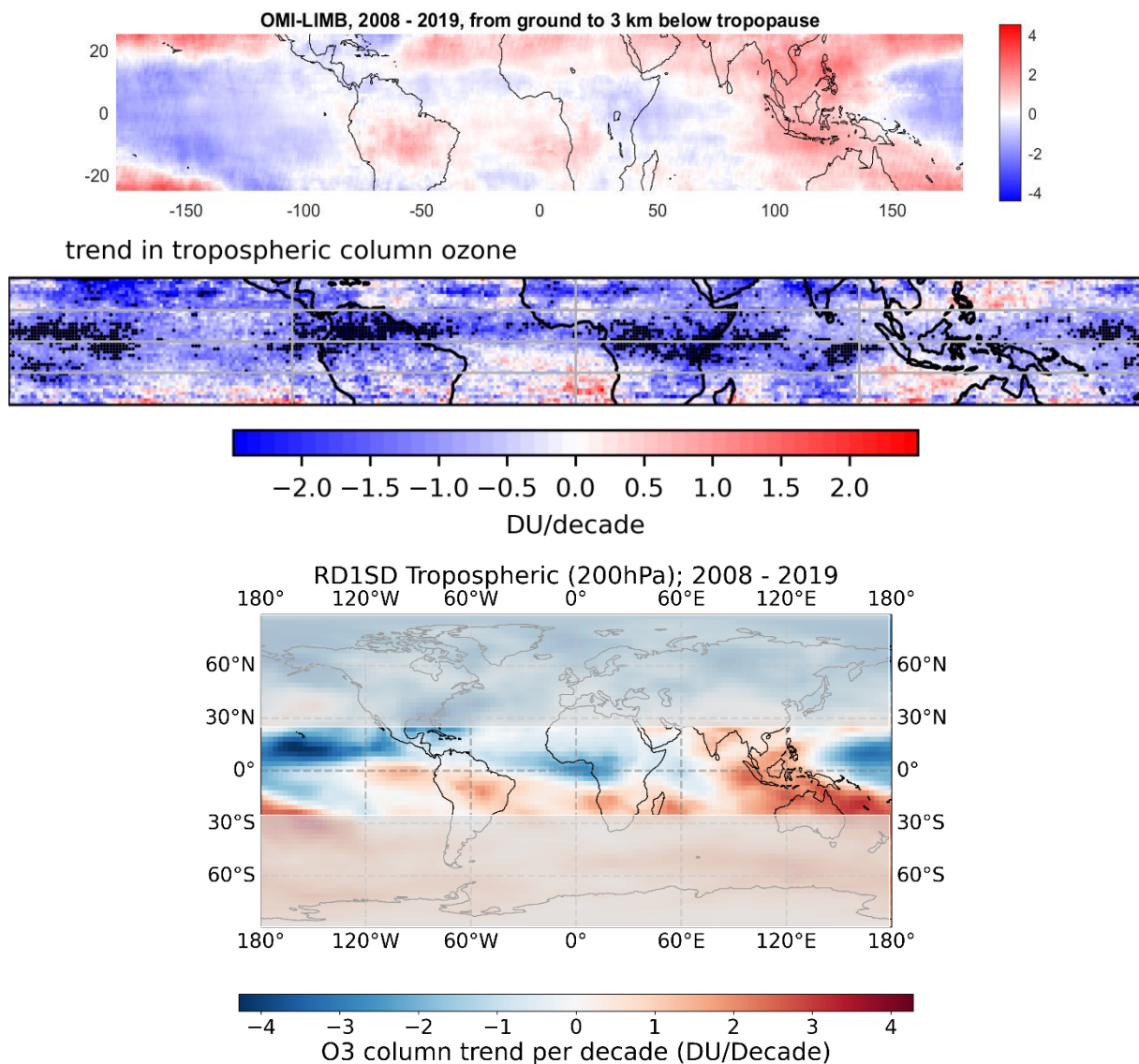
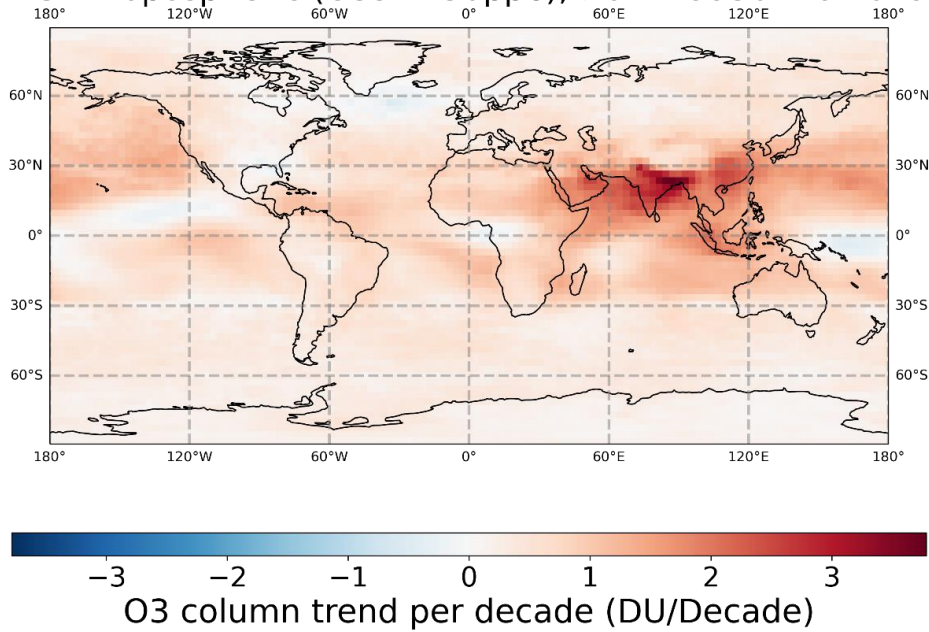


**Figure 18:** Comparison of the (Top) OMI-LIMB (TCO3 up to 3 km below the tropopause); (Middle) TTOC\_CCD (TCO3 up to 200 hPa); (Bottom) RD1SD CCM simulation (TCO3 up to 200 hPa) for the period from 2008 to 2019. The units are the same in all three images, i.e. DU/decade.

Finally, the three TCO3 data sets SUNLIT-OMI-LIMB, TTOC\_CCD and CCM EMAC RD1SD are compared concentrating of the tropical region (i.e. 20°S – 20°N) for the period from 2008 to 2019, for which all data sets are available (Figure 18). The derived TCO3 trends from OMI-LIMB and RD1SD agree quite well in terms of the change pattern and the magnitude of the DU per decade values. The trend patterns derived from the TTOC\_CCD agree in parts, for instance in the northern tropics over the Pacific, the southern Atlantic, but there are also large differences, for example over Brazil and Indonesia. Overall, the TCO3 trend values (in DU/decade) derived from the TTOC\_CCD are lower than those trend values derived from OMI-LIMB or RD1SD.

RD1SD Tropospheric (O3sm150ppb); from 199501 to 201912



RD1SD Tropospheric (O3sm150ppb); from 200501 to 201912

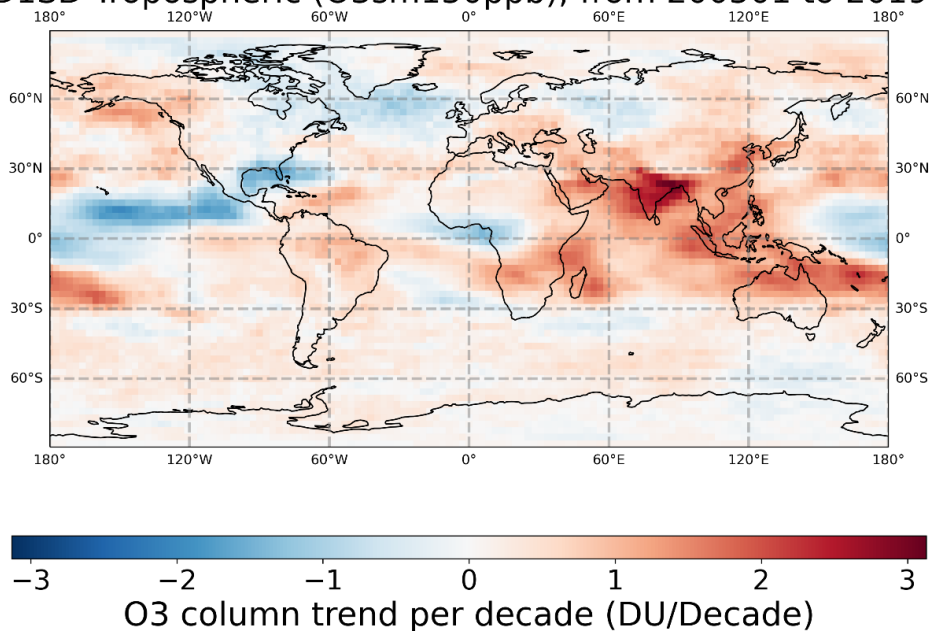


**Figure 19:** Trend analyses based on the CCM EMAC simulation RD1SD, here for the two different periods of 1995 – 2019 and 2005 – 2019, to be consistent with the ozone data trend analyses based on the two ESA ozone data products SUNLIT-OMI-LIMB TCO3 and TTOC\_CCD. This “specified dynamics” reference simulation (RD1SD) is nudged towards ERA-5 reanalysis data (monthly averages on T42, which is about  $2.8^\circ \times 2.8^\circ$  (latitude  $\times$  longitude)).

In conclusion, Figure 19 shows the corresponding tropospheric ozone column (TCO3) trend results based on the CCM EMAC RD1SD simulation with respect to the different periods (i.e. 1995 – 2019 and 2005 – 2019) for the discussion with the respective ESA Ozone\_cci data products, i.e. TTOC\_CCD and SUNLIT-OMI-LIMB. The definition of the TCO3 is based on the ozone mixing ratio threshold value of 150 ppbv, i.e. describing the ozonopause. Figure 19 indicates that the chosen

time period for the trend analysis is clearly influencing the trend values, in some regions even the signs of the trend change.

- Further CCM based (partial) TCO3 trend estimates

The paper by Fiore et al. (2022) focused on recent lower tropospheric ozone trends in the context of large internal variability. The study is based on multi-decadal simulations (in total 15-member ensemble) using the CCM CESM2-WACCM6 covering the period from 1950 – 2014. The analysis of tropospheric ozone trends is concentrating on the annual mean lower tropospheric ozone (from the surface to 690 hPa). The results from different ensemble members and for different time periods (i.e. 20 and 10 years) have been used to point out the role of internal variability. The results shown in Figure 20 indicate some similarities in terms of trend change patterns but also regions where the determined trends are very different.

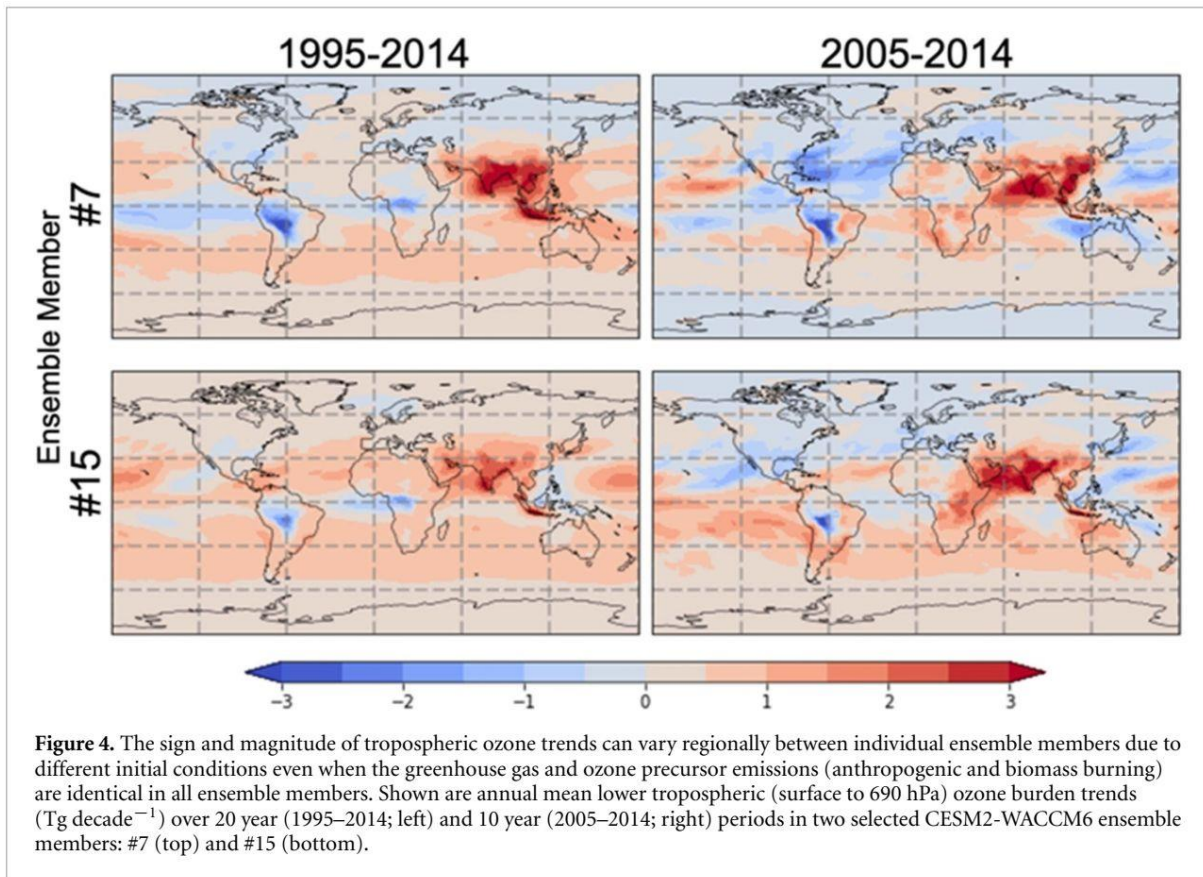
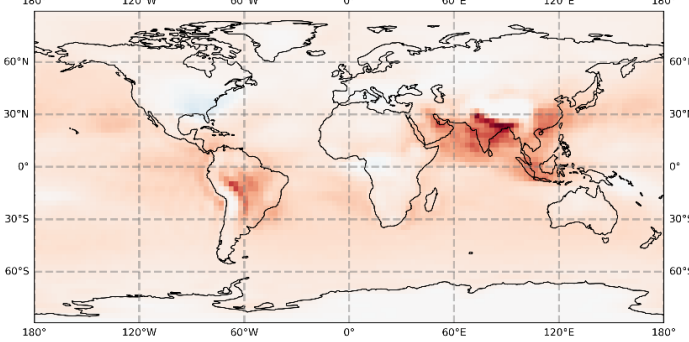


**Figure 20:** This is Figure 4 (incl. the original caption) taken over from Fiore et al. (2022). The results are from the CCM WACCM. Please note: the shown values are partial tropospheric ozone columns, which span the altitude range from the surface up to 690 hPa.

In general, the overall lower tropospheric ozone trend pattern presented in Figure 20 is looking similar between the different ensemble WACCM members and also for the two periods analyzed (1995 – 2014 and 2005 – 2014), for instance the strong positive trends over southeast Asia or the negative ozone trend over central South America (SA). The identified positive trend signal in southeast Asia is in line with the discussed TCO3 trends above but the negative lower troposphere ozone trend over SA seems to be in contradiction with the TCO3 results (for the entire troposphere) presented by Gaudel et al. (2018) and the other trend analyses discussed before including those of the CCM EMAC RD1SD simulation results. In order to enable a better comparison between WACCM and EMAC results, the RD1SD simulation trend analysis for the lower troposphere (surface to 690 hPa) were determined in the same way. Figure 21 is impressively showing that for the two periods 1995 – 2019 (middle part)

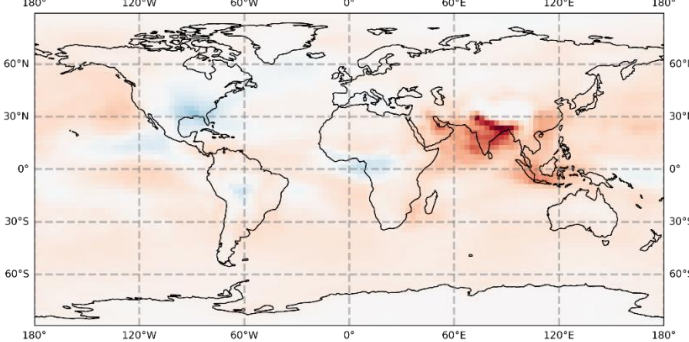
and 2005 – 2019 (low part) a negative trend is also found over SA in the lower troposphere. Obviously, the trend analysis performed for the longest time series based on RD1SD (1980 – 2019, top of Figure 21) indicate a positive trend over SA. This indicates strong ozone increases in the lower troposphere in this region in the 1980s and early 1990s.

RD1SD Tropospheric (690hPa); from 198001 to 201912



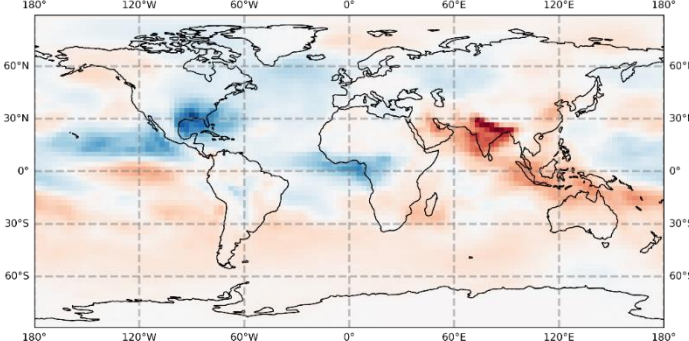
-1.5 -1.0 -0.5 0.0 0.5 1.0 1.5  
O3 column trend per decade (DU/Decade)

RD1SD Tropospheric (690hPa); from 199501 to 201912



-1.5 -1.0 -0.5 0.0 0.5 1.0 1.5  
O3 column trend per decade (DU/Decade)

RD1SD Tropospheric (690hPa); from 200501 to 201912



-1.5 -1.0 -0.5 0.0 0.5 1.0 1.5  
O3 column trend per decade (DU/Decade)

**Figure 21:** Lower tropospheric column ozone changes (partial column from the surface to 690 hPa) as derived from RD1SD for comparison with the WACCM results presented in Figure 20.

In this context, the TCO<sub>3</sub> trends (i.e. for the entire troposphere) derived from the CCM EMAC RD1SD simulation as shown in Figure 10 indicate different signs of trend over SA for the slightly shifted analyzed periods (i.e. 2003 – 2012 and 2005 – 2014), which is a strong hint that trend estimates for the troposphere based on 10 years only are not robust. The results presented in Figure 19 for longer periods (1995 – 2019 and 2005 – 2019) showing a more reliable trend patterns, in particular with respect to the trend results for SA, which are also in line with those presented in Figure 21 (i.e. trends in the lower troposphere). Such results point to out that the internal variability is relatively strong in comparison with the expected anthropogenic tropospheric ozone trends. Fiore et al. (2022) also stated that “even two-decade record length is insufficient to eliminate the role of internal variability, which can produce regional tropospheric ozone trends oppositely signed from ensemble mean (forced) changes.” The differences regarding the trend value as presented in Figure 20 can be large, they even partially change their sign (for instance in the North Atlantic, over the African continent). In this case, the presented results of EMAC are more stable, i.e. the trend patterns between the two analyzed periods are more stable (Figure 21).

In addition, the tropospheric ozone trend analyses presented in Fiore et al. (2022) based on WACCM show that

- the strongest positive tropospheric ozone trends (TCO<sub>3</sub>) are found in the subtropical regions (20° – 30°) with stronger trends in the northern hemisphere (Figure 22), independent of the chosen period (1950 – 2014, 1979 – 2005, 2005 – 2014); this statement is also valid for the corresponding TCO<sub>3</sub> trends from the CCM EMAC RD1SD simulation (Figure 21).
- The trend values for lower (greater than 690 hPa) and upper troposphere (380 hPa to tropopause) ozone derived for the period 1995-2014 both indicating strongest trends in the subtropics for the annual means, but also indicating a seasonal dependence (Figure 23).

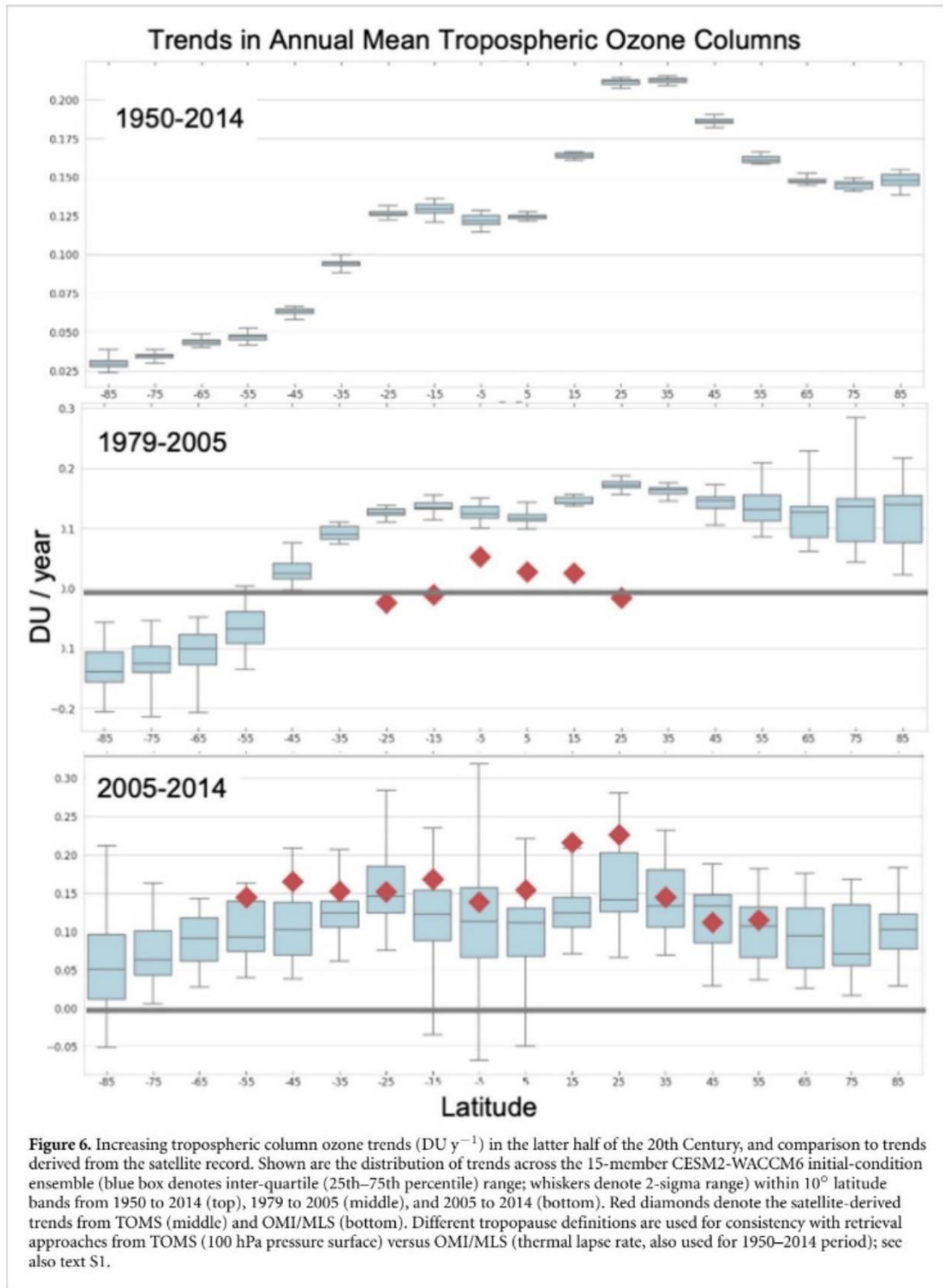


**Figure 22:** This is Figure 6 (including the original caption) taken over from Fiore et al. (2022). Comparison of WACCM results with observations (red diamonds) regarding TCO3 (the entire troposphere).

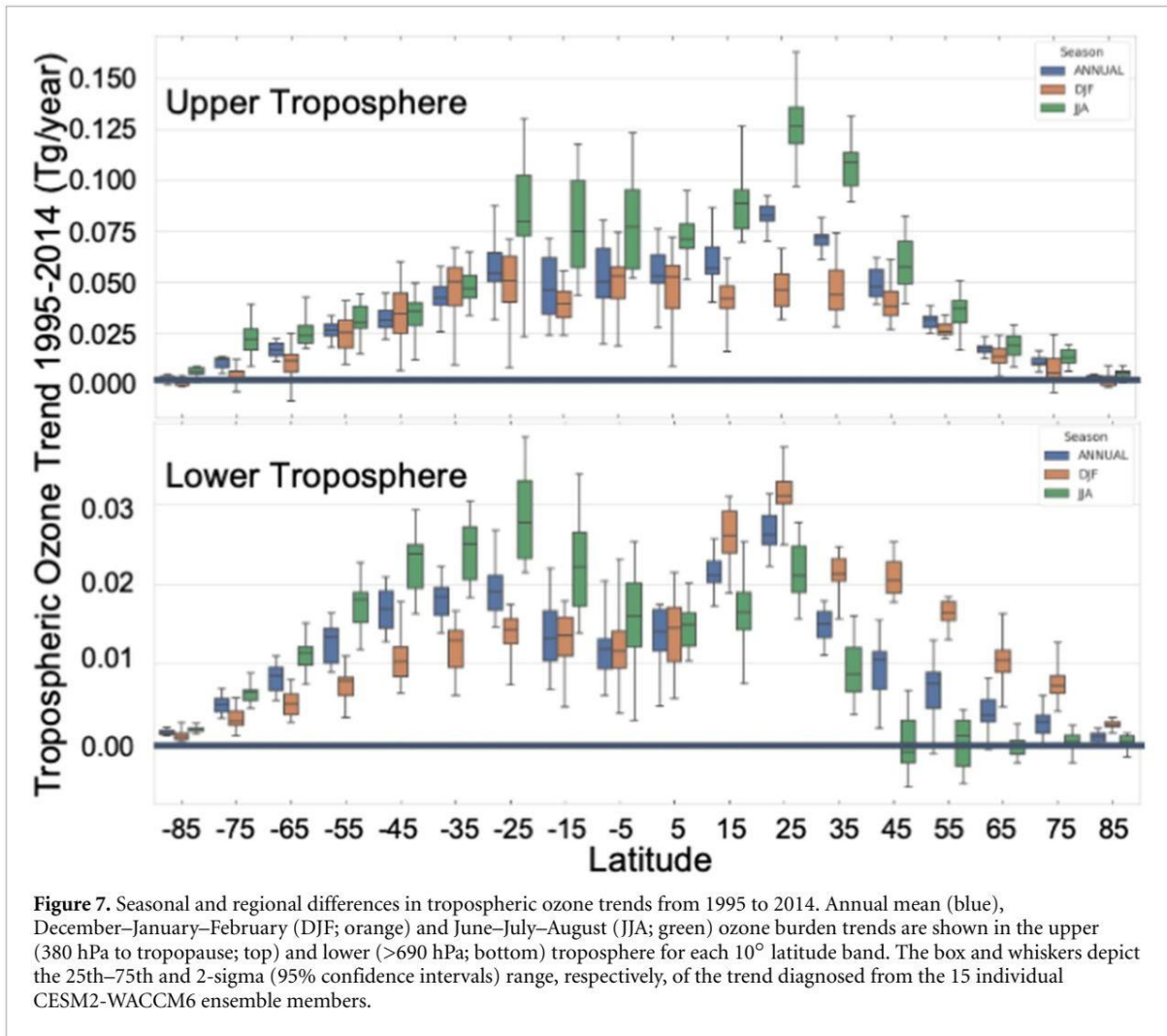


**Figure 23:** This is Figure 7 (including the original caption) taken over from Fiore et al. (2022).

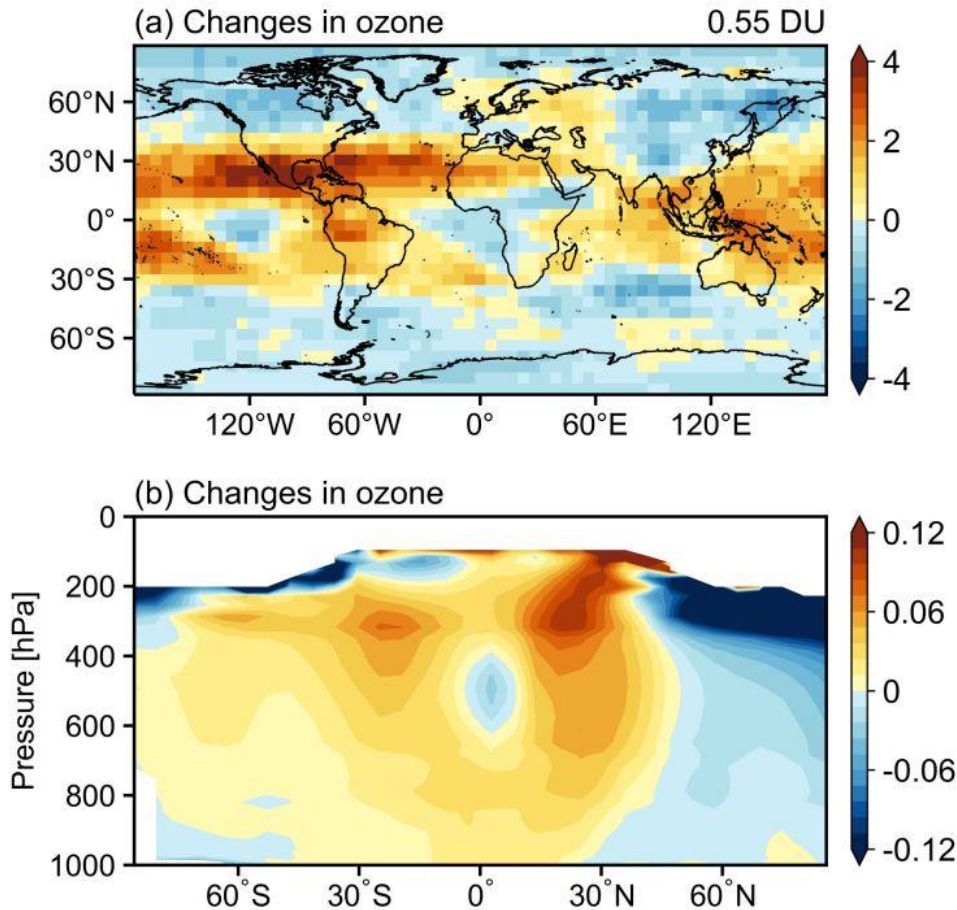
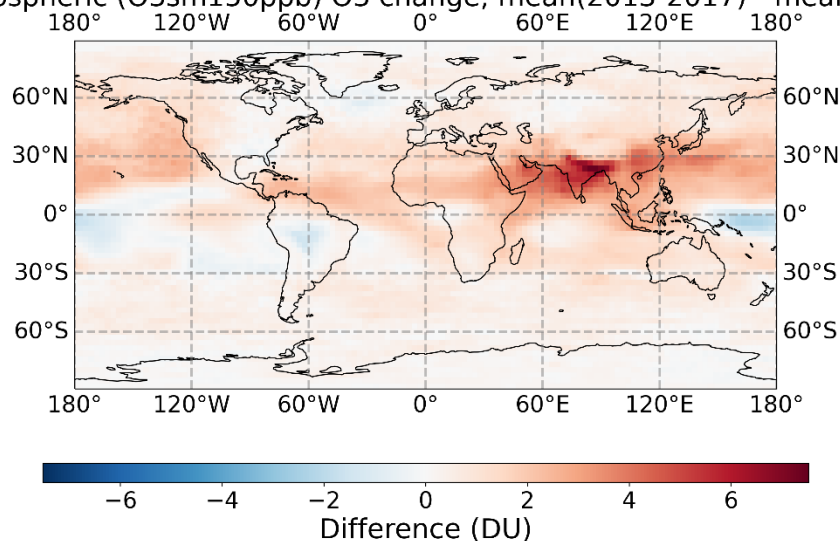


**Figure 24:** Parts (a) and (b) of Figure 12 taken over from Wang et al. (2022). It shows (a) differences in the modeled annual mean TCO<sub>3</sub> in Dobson Unit (DU) and (b) relative differences in the zonal mean ozone mixing ratio between the five-year means of 2013 – 2017 and 1995–1999.

By Wang et al. (2022), among others, a study is conducted looking at global tropospheric ozone trends in the period 1995 – 2017. The investigation is based on the IAGOS database, which were also compared with ozonesonde measurements and a multi-decadal GEOS-Chem chemical model simulation. The investigated GEOS-Chem simulation is driven by reanalysis meteorological fields and the most up-to-date year-specific anthropogenic emission inventory. In Figure 24, they considered 5-year averages in the comparison to reduce the impact of short-term climate variability on ozone. The modeled global average TCO<sub>3</sub> increased by 0.55 DU in 2013–2017 compared to the 1995–1999 level (Figure 24, part a), with the greatest increases in the (sub-)tropical upper troposphere (Figure 24, part b), where ozone radiative impacts are the largest. GEOS-Chem reproduces the overall pattern of observed tropospheric ozone trends, with strongest TCO<sub>3</sub> trends in the (sub-)tropics, i.e. the Pacific region and around Indonesia, which is in line with other climatological means as presented before. The absolute trends values are partly different. Figure 25 (top part) is showing the respective result as derived from the CCM EMAC RD1SD simulation. Even if the (sub-)tropics stand out in both images (i.e. GEOS-Chem and RD1SD), there are obvious differences in the spatial distribution, for instance in the East Pacific/Middle America/Atlantic regions or South America. The GEOS-Chem results are showing slightly higher positive trends in the northern and southern subtropics (note the different color bars), whereas the TCO<sub>3</sub> trends are slightly weaker over India.

RD1SD Tropospheric (O3sm150ppb) O3 change; mean(2013-2017) - mean(1995-1999)



RD1SD Tropospheric O3 Change; mean(2013-2017) - mean(1995-1999)

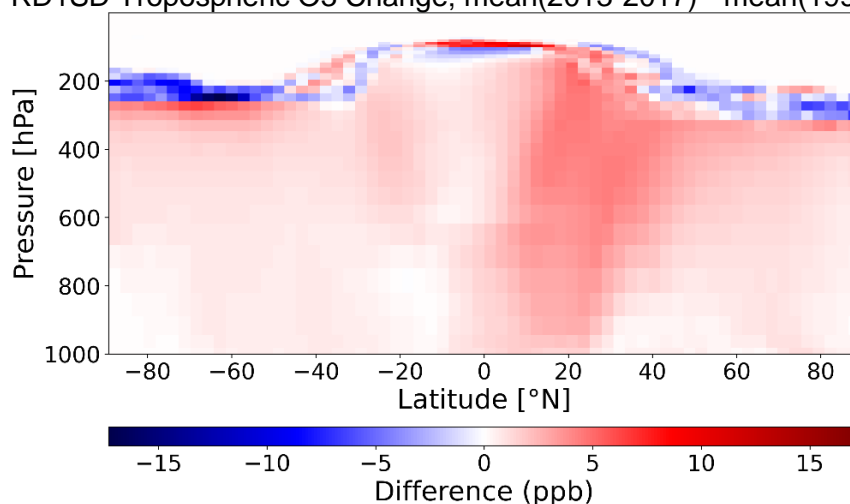


**Figure 25:** For direct comparison with the results shown in Figure 24, presented are (top) differences of the modeled annual mean TCO<sub>3</sub> (in Dobson Unit, DU) and (bottom) differences of the zonal mean ozone mixing ratio (in ppbv) between the five-year means of 2013– 2017 and 1995–1999 derived from the CCM EMAC RD1SD simulation.

In both models the vertical change pattern of the zonal mean tropospheric ozone between the 5-year means for the 2013 – 2017 and 1995 – 1999 periods look similar. The analysis of the two CCM simulations of GEOS-Chem (Figure 24, bottom) and of CCM EMAC RD1SD (Figure 25, bottom) both show the strongest trends in the subtropical regions in both hemispheres. They are more pronounced in the northern hemisphere and they also reach here down to the surface; the biggest changes are found in the upper part of the troposphere. For the mid-latitudes of the southern hemisphere both models are indicating enhanced ozone of similar magnitude, whereas the results for the northern hemisphere mid-latitudes are looking different. The analysis of GEOS-Chem results is showing a negative ozone trend in all altitudes, whereas EMAC RD1SD is indicating a positive ozone trend throughout the troposphere.

The study prepared by Pope et al. (2023) is investigating the spatial and temporal variability of ozone in the lower troposphere as derived from the RAL Space UV-Vis satellite products. Here the lower tropospheric ozone column (LTCO<sub>3</sub>) is defined for the height region from the surface up to 450 hPa.

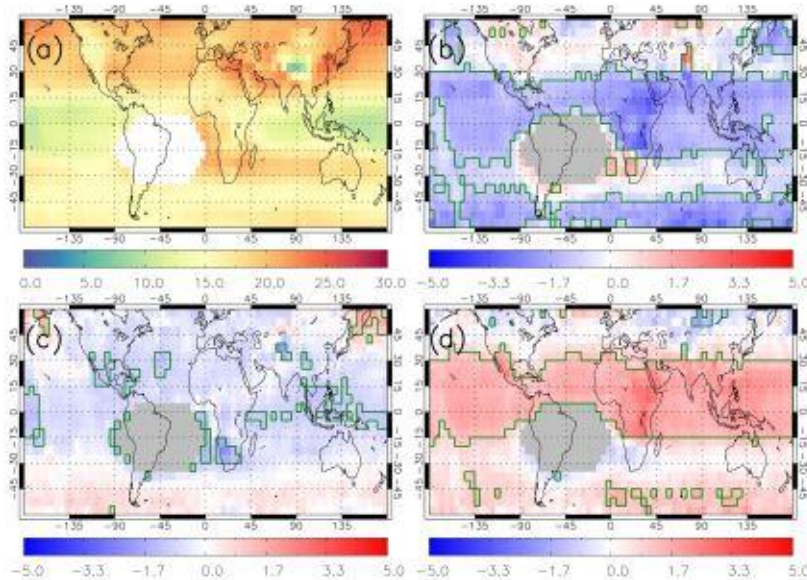


**Figure 7.** LTCO<sub>3</sub> (DU) merged data set from GOME-1 (1996–2002), SCIAMACHY (2003–2004) and OMI (2005–2017): (a) 1996–2017 long-term average, (b) 1996–2000 average anomaly, (c) 2005–2009 average anomaly and (d) 2013–2017 average anomaly. Anomalies are relative to the long-term average (a). Green polygon-outlined regions show substantial anomalies (95 % confidence level and where the absolute anomaly > 1.0DU) from the long-term average using the Wilcoxon rank test. White/grey pixels are where the South Atlantic Anomaly influence on retrieved LTCO<sub>3</sub> has been masked out.

**Figure 26:** This is Figure 7 (including the original caption) taken over from Pope et al. (2023).

Figure 26 (part a) is showing the climatological mean of the LTCO<sub>3</sub> for the period from 1996 to 2017 determined by RAL. The other three illustrations (part b, c, and d) are indicating the averaged anomalies for 1996 – 2000, 2005 – 2009, and 2013 – 2017. For comparison, in Figure 27 the corresponding results from the CCM EMAC RD1SD simulation are presented. The first thing that strikes you is that the climatological means for 1996 – 2017 look very similar, qualitative (the distribution pattern) and quantitative. Furthermore, it is noticeable that the change pattern of the 5-year average anomalies is changing in the same way, from mostly negative LTCO<sub>3</sub> anomalies for the period 1996 – 2000 to mostly positive LTCO<sub>3</sub> anomalies for the period 2013 – 2017. In the CCM EMAC RD1SD data the strength of the change is most pronounced over the Indian continent and Indonesia, whereas a more uniform change of the averaged anomalies is identified in the tropical and subtropical regions in the RAL data.

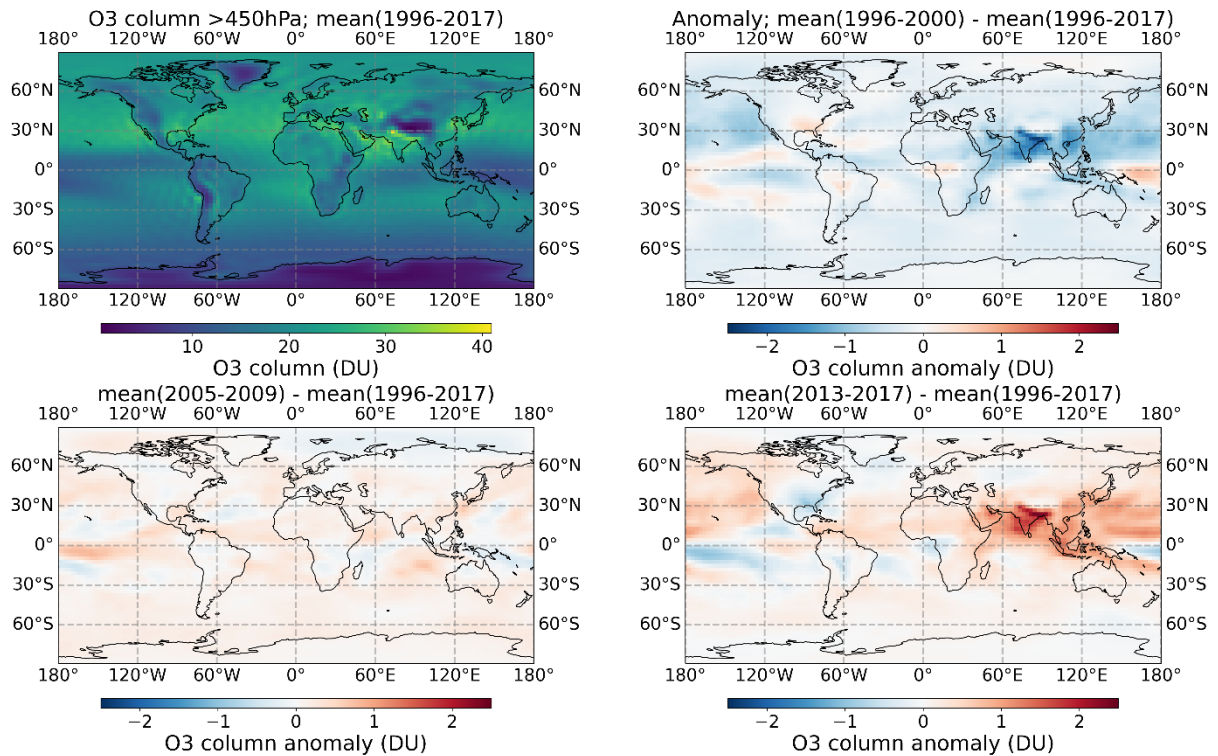


**Figure 27:** Presented are the corresponding LTCO<sub>3</sub> (surface – 450 hPa tropospheric sub column) results derived from the CCM EMAC RD1SD simulation. This figure has been prepared for comparison with the LTCO<sub>3</sub> product as derived from RAL Space UV-Vis satellite product (see Pope et al., 2023, see Figure 26, i.e. their Fig. 7).

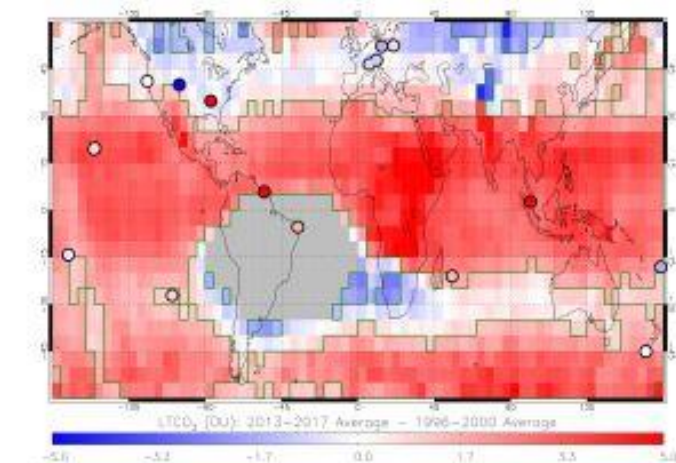


**Figure 8.** LTCO<sub>3</sub> (DU) merged data set from GOME-1 (1996–2002), SCIAMACHY (2003–2004) and OMI (2005–2017) where the difference between the 2013–2017 average and 1996–2000 average is shown. Green polygon-outlined regions show substantial differences (95% confidence level and where the absolute difference > 1.0 DU) using the Wilcoxon rank test. Grey pixels are where the South Atlantic Anomaly influence on retrieved LTCO<sub>3</sub> has been masked out. Circles show differences in ozonesonde LTCO<sub>3</sub> (DU) over the same time periods as the merged satellite record.

**Figure 28:** This is Figure 8 (including the original caption) taken over from Pope et al. (2023).

RD1SD Tropospheric (450hPa) O<sub>3</sub> change; mean(2013-2017) - mean(1996-2000)

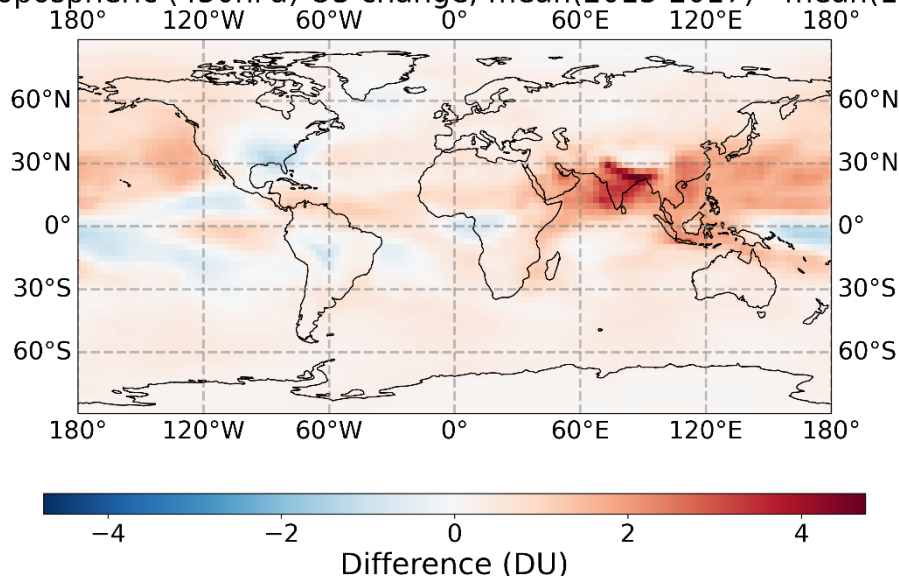
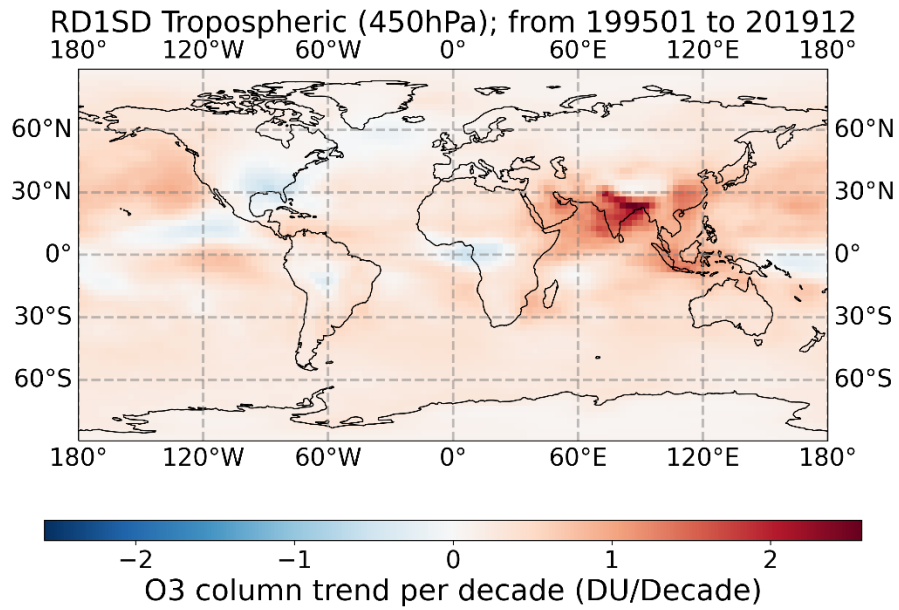


**Figure 29:** Presented are the LTCO<sub>3</sub> (surface – 450 hPa tropospheric sub column) differences between the 1996 – 2000 and 2013 – 2017 5-year averages (in Dobson Units) based on the CCM EMAC RD1SD simulation. This figure has been prepared for comparison with the LTCO<sub>3</sub> product as derived from RAL Space UV-Vis satellite product (see Pope et al., 2023, see Figure 28, i.e. their Fig. 8).

Based on the two data sets of the RAL Space UV-Vis satellite product and the CCM EMAC RD1SD simulation the difference between the 2013 – 2017 average and the 1996 – 2000 averaged LTCO<sub>3</sub> have been calculated. The results are presented in Figure 28 (for RAL Space UV-Vis) and in Figure 29 (for RD1SD). Some matching results are found, in particular strongest changes in LTCO<sub>3</sub> are identified in the (sub-)tropics (30°N – 30°S), with mostly pronounced (positive) changes over India and Indonesia. Moreover, negative ozone changes are seen over the North-Eastern American continent (all the way down to Florida) and positive ozone changes in the North-Pacific region. Differences in the results can be found in the mid-latitude regions: The RAL data show regions with clear negative changes in the northern hemisphere and strong positive changes in the southern hemisphere. The CCM EMAC RD1SD indicates here low positive ozone changes in both mid-latitude regions.



**Supplement to Figure 29:** For comparison with Figure 29, the calculated linear trend of LTCO<sub>3</sub> for the period 1995 – 2019 from the EMAC-RD1SD simulation. The trend pattern is looking very similar, but the strength of the regional trends is different (maximum values are much lower; see the different color bars).

## 5. TCO3 trend analyses in different latitudinal regions

The aim here is to derive latitude-dependent TCO3 trends and classify them in comparison to natural (internal) variability. The analyses carried out are based on the TCO3 values derived from SUNLIT-OMI-LIMB and from the CCM EMAC RD1SD simulation, respectively.

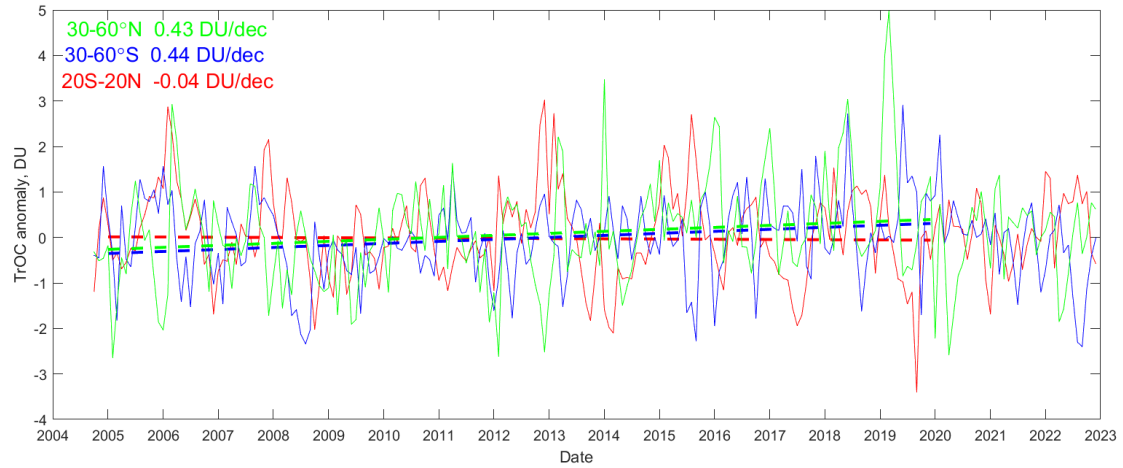


**Figure 30:** SUNLIT-OMI-LIMB TCO3 data deseasonalized anomalies (solid lines) and trends (dashed lines). Trends shown in the plot are estimated using quantile regression, for years 2005 – 2019.

**Table 1:** Different TCO3 trend estimates based on the SUNLIT-OMI-LIMB for years 2005 – 2019 using various methods.

	Quantile regression	Multiple linear regression (linear, solar, QBO, ENSO)	Simple linear fit years 2005-2019	Difference 2016-2020 minus 2005-2008
20°N-20°S	- 0.04 DU/dec	- 0.24 DU/dec	- 0.21 DU/dec	- 0.25 DU/dec
30°S-60°S	0.44 DU/dec	0.50 DU/dec	0.37 DU/dec	0.43 DU/dec
30°N-60°N	0.43 DU/dec	0.84 DU/dec	0.87 DU/dec	0.64 DU/dec

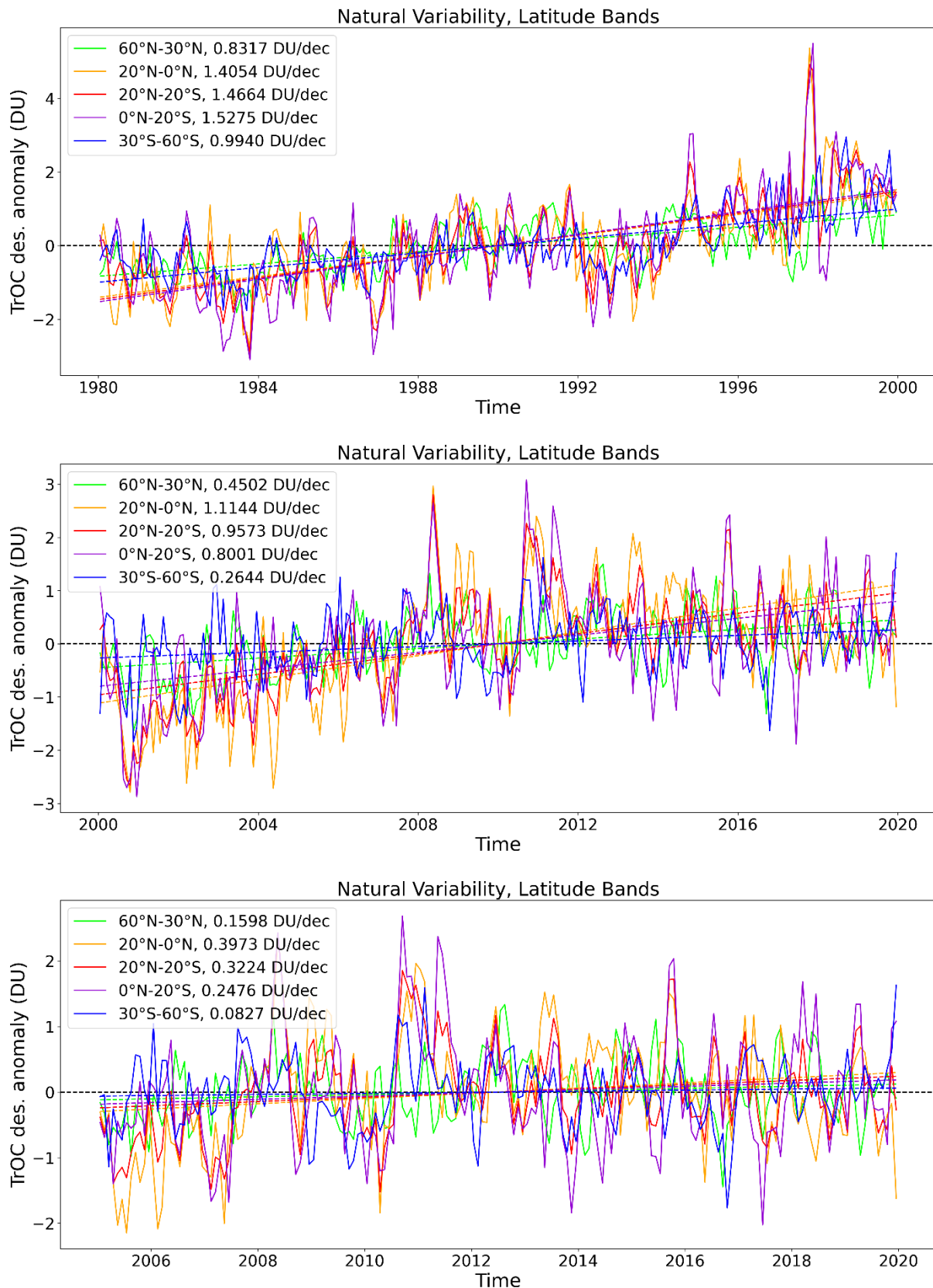


**Figure 31:** TCO3 trend analysis based on the RD1SD CCM simulation. Top: 1980-1999, middle: 2000-2019, bottom: **2005-2019**. Ozonopause: threshold value 150 ppbv; weighted mean per latitude band using grid area; Anomaly: Subtract mean value over time series; deseasonalized: Subtract mean value per month over time series: Latitude Bands: 60°N – 30°N, 20°N – 20°S, 30°S – 60°S; Additional Bands: 20°N – 0°N, 0°N – 20°S.

Based on the results of the CCM EMAC RD1SD simulation (from 1980 – 2019), the TCO<sub>3</sub> trends of different latitudinal bands and time periods have been determined. For comparison, we have looked at the analysis based on the SUNLIT-OMI-LIMB TCO<sub>3</sub> data set (Table 1 and Figure 30; period from 2005 – 2019, referred to as “observations” in the following). The respective CCM EMAC RD1SD results (see the Figure 31 bottom part) anomaly plots (in DU) with the corresponding trend values (in DU/decade) are indicating differences regarding the latitudinal trends from observations and also the individual strength of the trends. The determined natural variability of the model results and observations has the same order of magnitude.

Here are the major points regarding the comparison (i.e. the match of the model data and observations and obvious differences):

1. The model data (CCM EMAC RD1SD) and observations (SUNLIT-OMI-LIMB) are indicating a similar range of natural TCO<sub>3</sub> variability, i.e. in the order of +/- 3 DU. Mid-latitudinal regions (30° – 60°N and S) and the tropics (20° – 20°N/S) are indicating the same behavior regarding the (natural) variability.
2. The long-term behavior of TCO<sub>3</sub> from SUNLIT-OMI-LIMB are not showing a similar behavior as found from RD1SD model data, i.e. a positive trend before year 2010; afterwards there are no obvious trends detected, similar with SUNLIT-OMI-LIMB TCO<sub>3</sub> data.
3. For the time period of **2005 – 2019** the TCO<sub>3</sub> trend values (here using a simple linear fit) are showing obvious differences:
  - a. NH mid-lat.: **0.87** DU/dec (obs) vs. **0.16** DU/dec (model) [explanation: obs are showing a clear positive trend north of about 40°N, for instance in the North Atlantic region, which is not identified in the RD1SD trend estimates];
  - b. SH mid-lat.: **0.37** DU/dec (obs) vs. **0.08** DU/dec (model) [explanation: obs are showing a clear positive trend south of about 40°S, which is not identified in the RD1SD trend estimates];
  - c. There is a match between obs and model, i.e. that the NH is showing higher trend values than in the SH, which seems to be realistic. But the model trends are clearly much weaker (only about 10%).
  - d. Tropics: **- 0.21** DU/dec (obs) vs. **0.32** DU/dec (model) [explanation: obs are indicating an obvious negative trend in the tropical region, whereas the RD1SD is showing a positive trend in this region. Beside a positive trend over South-East Asia/China, both in obs and the model, over and beyond the RD1SD is showing clear positive trends in the Indian continent region, over Indonesia and Northern Australia, which are not identified in the obs].
  - e. The model is showing the most obvious trends in the tropics whereas the observational data (SUNLIT-OMI-LIMB) are indicating clearer trends at mid-latitudes (in both hemispheres). The CCM EMAC RD1SD results are generally in better agreement with other published analyses (e.g. Gaudel et al., 2018; Ziemke et al., 2019; Fiore et al., 2022; Wang et al., 2022).
4. Comparing the time periods **1980 – 1999 and 2000 – 2019** (model only):

The trend values are all stronger for the time period 1980 – 1999 in comparison with 2000 – 2019 (in mid-latitudes and tropics). More or less steady positive trends can be seen from 1980

until end-2000, but after about year 2008 there are no clear trends visible. Again, the calculated trend values in the tropics are higher in comparison the mid-latitude values.

Trend analysis of TCO<sub>3</sub> is obviously time-consuming and difficult because the detected trend values are in the same order of magnitude as the natural (internal) variability.

## 6. Summary discussion

Comprehensive, continuous and consistent long-term ozone data records (over a few decades) derived from different satellite instruments are important to create a complete picture of the global ozone distribution and its temporal and spatial changes in the troposphere and stratosphere. Long-lasting time series of ozone at a global scale are needed to monitor atmospheric ozone as well as for the evaluation of global chemistry-climate model simulations. High quality ozone data records are essential to enable confident ozone trend analyses. This is a challenge, in particular for the detection of appropriate and reliable trends of tropospheric ozone (TCO3), since its natural (internal) variability has the same order of magnitude as the expected long-term changes due to man-made activities. At this point considering the results of chemistry-climate models can help clarifying differences in ozone data sets from space-borne observations.

### *TCO3 climatological means*

The various TCO3 climatologies available, including those created as part of the ESA Ozone\_cci project, are looking sometimes very different (see Figures 2 and 3). This then makes it more difficult to derive reliable trends in tropospheric column ozone. One possible reason for that is that the applied retrieval methods to derive the corresponding tropospheric ozone data products are using different requirements and preliminary information or other boundary conditions, which strongly affect the data. In addition, the creation of consistent time series for longer periods (years to decades) represents a challenge because the used time series originate from different measuring systems.

Another reason for the differences of the published TCO3 climatologies (e.g. in the TOAR; see Figure 2) is that the analyses often have been based on relatively short time series of data (in this case only five years). In principle it does not allow the TCO3 trends to be reliably determined. It must be also noted that when TCO3 climatologies that are based on relatively short periods of time, the length of the time series is also crucial with regard to the derived TCO3 distribution.

The shown comparisons of the different ozone climatologies for the troposphere indicate that an exact determination of the tropopause (for instance using the WMO 2 K/km lapse-rate tropopause height, or fixed pressure levels) or of the upper boundary of the TCO3 (a determination related to a specific mixing ratio, i.e. defining a so-called ozonopause) only plays a subordinate role. Although this may lead to slighter differences in the TCO3 values, it does not affect climatological patterns.

Although the TCO3 distribution patterns differ significantly in some cases, there are regions where the climatologies are (mostly) showing the same pattern: For instance, low TCO3 values are always found over Indonesia and the West Pacific region. High TCO3 values are usually identified in the northern and southern subtropics, in particular over East Asia and the South Atlantic off the African continent. What also often catches the eye is the East-West gradient of the TCO3 across North and South America, which are closely connected with the large mountain ranges, i.e. the Rocky Mountains and the Andes.

In conclusion, it can be said the regions mentioned are most suitable for corresponding checks using other measurement data (e.g. ground based or ozonesonde measurements), but also for comparisons with model results. The TCO3 climatologies created as part of the ESA Ozone\_cci project (i.e. SUNLIT-OMI-LIMB and TTOC\_CCD) mostly agree. The ozone distribution patterns confirm the results of previously published ozone climatologies (e.g. in the TOAR). It should be noted that the database is as similar as possible (i.e. in terms of the length of the data series) in order to ensure good comparability of different ozone data. It can be noted that the ESA ozone data sets for the troposphere turned out to be reliable.

The CCM EMAC used in this context (i.e. the RD1SD simulation) confirms the general tropospheric ozone distribution pattern.

### *TCO3 trend estimates*

Robust trend estimates of the tropospheric ozone column (TCO3) values are difficult because the internal, natural fluctuations of TCO3 (in the order of 2-3 DU) is of the same order of magnitude as the determined TCO3 trends (2-3 DU/decade). For this reason, tropospheric ozone time series as long as possible (preferably longer than 10 years) are needed. If tropospheric ozone trends are derived from short time series (less than 10 years), then no reliable trends can be determined; in some cases, even the sign sometimes differs in such analyses.

The published trend analyzes of the TCO3 (especially in the TOAR) reveal some individual regions that show stable positive trend patterns, which are confirmed by ESA's CCI tropospheric ozone data. In particular, areas in the tropics, especially Brazil (Amazonas region) and Indonesia to North Australia, are indicating positive TCO3 trends. Clear negative TCO3 trends are determined in the tropical Pacific region. The results based on the CCM EMAC RD1SD simulation confirm these findings. It turned out that by using the same tropospheric ozone column thicknesses (i.e. the same definition of the upper edge of the troposphere), the trend estimates based on different data sets sometimes agree better.

The analysis of zonal mean TCO3 trends in specific regions (i.e. mid-latitudes and tropics) derived from the SUNLIT-OMI-LIMB data set for the period from 2005 to 2019 shows a different picture with stronger positive trends in the extra-tropical regions and very low trends in the tropics. After the detection of a change in the strength of the TCO3 trends at all latitudes around the year 2008 in the data derived from the CCM EMAC RD1SD simulation (i.e. with stronger positive TCO3 trend before 2008), this finding was confirmed by the analysis of the TTCO\_CCD data set (1995-2019), by dividing the data set into two parts, i.e. from 1995 to 2007 and 2008 to 2019. With the focus of the tropical region, especially the SUNLIT and EMAC data matches very well (and to a limited extent also with TTCO) with respect to the trend pattern for the period from 2008 to 2019 and which are in good agreement with the trend estimates published in TOAR.

One final note: The CCM EMAC RD1SD simulation results can reproduce most observation-based results (climatological mean TCO3 values as well as the TCO3 trends) quite well. They also show reliable (consistent) results in regions that are poorly documented by measurements, for example at high (polar) latitudes. Additionally, the results derived from a CCM can be used to illustrate and explain differences between datasets derived from observations.

## 7. Addition: A short summary of recent findings presented in WMO (2022)

To finalize this CAR, a brief summary of the key findings of the recent “WMO Scientific Assessment of Ozone Depletion: 2022” is presented. These updates and supplements the last CAR (Dameris et al., 2022).

Results of the work carried out in the ESA Ozone\_cci project made crucial contributions to the last WMO ozone assessment report (WMO, 2022; see also the CAR, which was prepared in the 3<sup>rd</sup> phase of the ESA Ozone\_cci Project). Among other, several scientific papers have been published in peer-reviewed journals in advance (e.g. Coldewey-Egbers et al., 2020; 2022; Dameris et al., 2021; Hubert et al., 2021; Sofieva et al., 2021; 2022; Weber et al., 2022).

In the ozone assessment report particular attention was paid to the strikingly high dynamic variability of the stratosphere, especially of the polar regions (i.e. Antarctic and Arctic) in recent years, which are characterized by strong (cold) and weak (warm) polar vortices as well as corresponding low and high stratospheric ozone contents. Clear statements can be found with respect to the future evolution of the total ozone content in the atmosphere, in particular regarding the attribution of total column ozone (TCO) trends during the period of slow ozone-depleting substances (ODSs) decline, which requires knowledge of changes in ozone in both the troposphere and stratosphere.

The most important statements (i.e. highlights) and key points on the recent and expected future evolution of the ozone layer globally and especially in polar regions are summarized below, taken from WMO (2022):

### Highlights:

- Actions taken under the Montreal Protocol continued to decrease atmospheric abundances of controlled ODSs and advance the recovery of the stratospheric ozone layer.
- Actions taken under the Montreal Protocol continue to contribute to ozone recovery. Recovery of ozone in the upper stratosphere is progressing. TCO in the Antarctic continues to recover, notwithstanding substantial interannual variability in the size, strength, and longevity of the ozone hole. Outside of the Antarctic region (from 90°N to 60°S), the limited evidence of TCO recovery since 1996 has low confidence.
- Outside of the polar regions, observations and models agree that ozone in the upper stratosphere continues to recover. In contrast, ozone in the lower stratosphere has not shown signs of recovery. Models simulate a small recovery in mid-latitude lower-stratospheric ozone in both hemispheres that is not seen in observations.

### Key results on polar ozone:

- Recovery of Antarctic stratospheric ozone continues to progress. Evidences have been found that September is the period when stratospheric ozone over Antarctica shows the largest sensitivity to decreasing ODSs.
- The 2019 ozone hole was the smallest since 2002. In contrast, both 2020 and 2021 had relatively large and long-lasting late spring ozone holes (see also Figure 32). (Annotation: 2022 and 2023 also showed persistent polar vortices in the southern hemisphere with low ozone values until late spring.)

- In the Arctic, observed trends in ozone remain small compared to the large year-to-year variability. No statistically significant signature of recovery in Arctic stratospheric ozone over the 2000–2021 period has yet been detected.
- Arctic total ozone reached exceptionally low values in spring 2020 (see also Figure 32).
- The broad range of polar springtime TCO in recent years in both hemispheres is largely explained by differences in the magnitude of the dynamical forcing.
- Future ozone depletion will be substantial in the Arctic during cold winters/springs as long as ODS concentrations are well above natural levels.
- Polar vortex trends and variability: The recent extreme polar vortex events in both hemispheres caused strong variations of polar ozone. However, currently there is no evidence for a systematic trend toward more frequent polar vortex disruptions in either hemisphere.

#### Key results on global ozone:

- Aggregated ground- and space-based observations indicate an increase of 0.3% decade<sup>-1</sup> in near-global (60°S–60°N) total column ozone over the 1996–2020 period. This trend is consistent with model simulations and our scientific understanding of the processes controlling ozone.
- Measurements show increases in upper stratospheric ozone for 2000–2020 outside of the polar regions. This is due to a combination of decreases in ozone-depleting substances and decreases in stratospheric temperature driven by increases in greenhouse gases (in particular CO<sub>2</sub>).
- Observations suggest small decreases in lower stratospheric ozone in the mid-latitudes of both hemispheres for 2000–2020, while chemistry-climate model simulations suggest small increases.
- Outside of polar regions, attribution of total column ozone trends during the period of slow ODS decline requires knowledge of changes in ozone in both the troposphere and stratosphere.
- For scenarios that assume strong reductions in the emission of tropospheric ozone precursors, the resulting reductions in tropospheric ozone can be important for total column ozone trends.
- Exceptional events (e.g. wildfires, strong volcanic eruptions) can temporarily perturb chemical and dynamical processes that affect stratospheric ozone amounts.

The given statements indicate that further monitoring of the atmosphere, especially ozone levels in the stratosphere and troposphere, is very important.

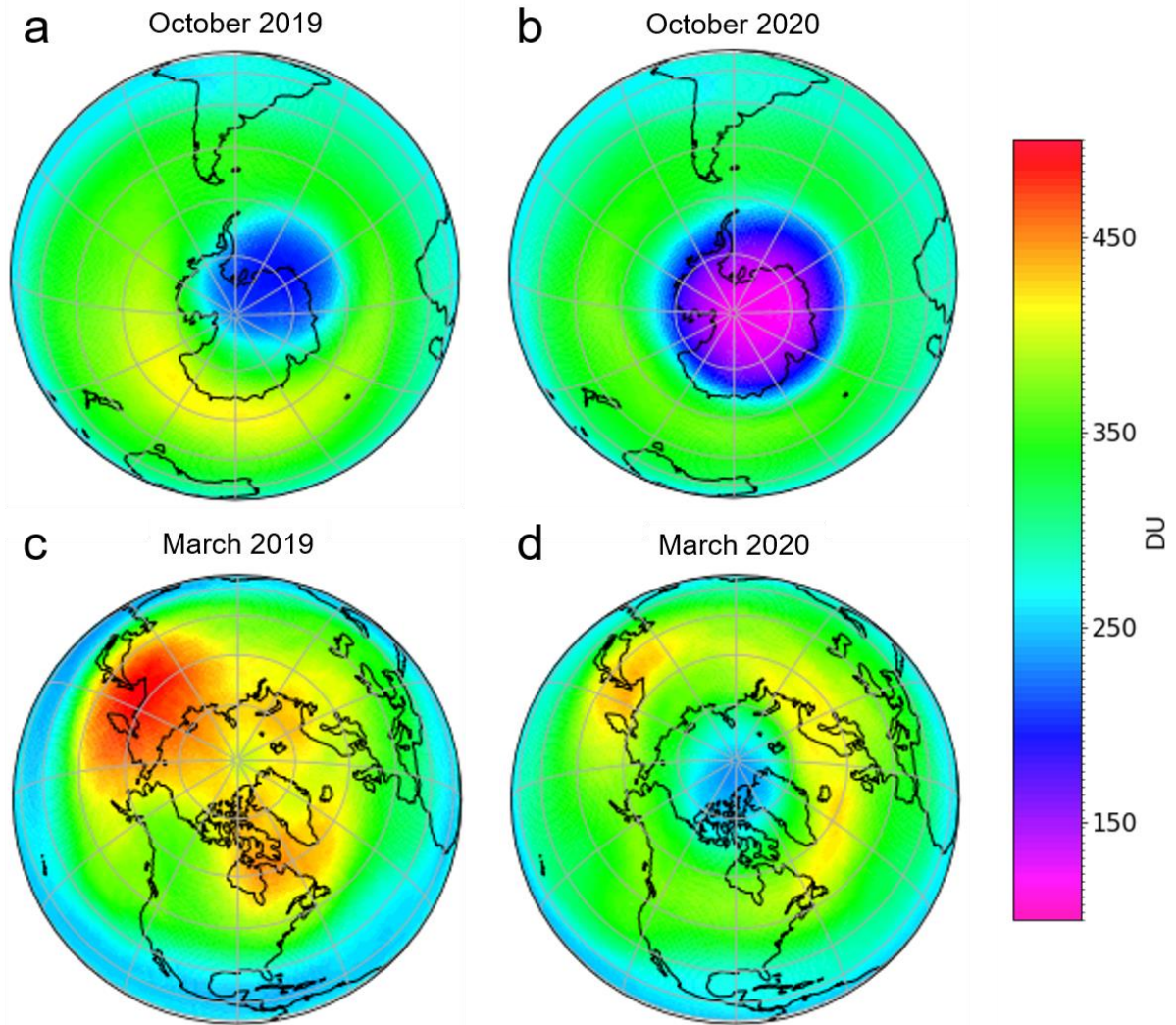


**Figure 32:** Representation of the TCO (in Dobson units, DU) in the southern polar region (parts a and b) and the northern polar region (parts c and d) in the respective months of October and March for the years 2019 (parts a and c) and 2020 (parts b and d). This false color view shows monthly averaged TCO values over the respective polar regions. Low ozone values are shown in blue and purple and high ozone levels are shown in orange and red (Data source: Copernicus Climate Change Service, 2020).

## References

- Christiansen, A., Mickley, L. J., Liu, J., Oman, L. D., and Hu, L.: Multidecadal increases in global tropospheric ozone derived from ozonesonde and surface site observations: can models reproduce ozone trends? *Atmos. Chem. Phys.*, 22, 14751–14782, <https://doi.org/10.5194/acp-22-14751-2022>, 2022.
- Coldewey-Egbers, M., Loyola, D.G., Labow, G., and Frith, S.M.: Comparison of GTOECV and adjusted MERRA-2 total ozone columns from the last 2 decades and assessment of interannual variability, *Atmos. Meas. Tech.*, 13, 1633–1654, doi:10.5194/amt-13-1633-2020, 2020.
- Coldewey-Egbers, M., Loyola, D. G., Lerot, C., and Van Roozendaal, M.: Global, regional and seasonal analysis of total ozone trends derived from the 1995–2020 GTO-ECV climate data record, *Atmos. Chem. Phys.*, 22, 6861–6878, <https://doi.org/10.5194/acp-22-6861-2022>, 2022.
- Copernicus Climate Change Service, Climate Data Store: Ozone monthly gridded data from 1970 to present derived from satellite observations. Copernicus Climate Change Service (C3S) Climate Data Store (CDS), doi: 10.24381/cds.4ebfe4eb (Accessed on 10-11-2023), 2020.
- Dameris, M., Loyola, D. G., Nützel, M., Coldewey-Egbers, M., Lerot, C., Romahn, F., and van Roozendaal, M.: Record low ozone values over the Arctic in boreal spring 2020, *Atmos. Chem. Phys.*, 21, 617–633, <https://doi.org/10.5194/acp-21-617-2021>, 2021.
- Dameris, M., Coldewey-Egbers, M., van Weele, M.: Climate Assessment Report (CAR), ESA O<sub>3</sub>-CCI Project, D5.1 CAR, 42pp., [https://climate.esa.int/media/documents/CAR\\_Ozone\\_CCI\\_final\\_March\\_7\\_2022.pdf](https://climate.esa.int/media/documents/CAR_Ozone_CCI_final_March_7_2022.pdf), 2022.
- Fiore, A. M., Hancock, S. H., Lamarque, J.-F., Correa, G. P., Chang, K.-L., Ru, M., Cooper, O., Gaudel, A., Polvani, L. M., Sauvage, B., and Ziemke, J. R.: Understanding recent tropospheric ozone trends in the context of large internal variability: a new perspective from chemistry-climate model ensembles, *Environ. Res.: Climate*, 1, 025008, <https://doi.org/10.1088/2752-5295/ac9cc2>, 2022.
- Gaudel, A., Cooper, O. R., Ancellet, G., Barret, B., Boynard, A., Burrows, J. P., Clerbaux, C., Coheur, P. F., Cuesta, J., Cuevas, E., Doniki, S., Dufour, G., Ebojje, F., Foret, G., Garcia, O., Granados-Muñoz, M. J., Hannigan, J. W., Hase, F., Hassler, B., Huang, G., Hurtmans, D., Jaffe, D., Jones, N., Kalabokas, P., Kerridge, B., Kulawik, S., Latter, B., Leblanc, T., Le Flochmoën, E., Lin, W., Liu, J., Liu, X., Mahieu, E., McClure-Begley, A., Neu, J. L., Osman, M., Palm, M., Petetin, H., Petropavlovskikh, I., Querel, R., Rapp, N., Rozanov, A., Schultz, M. G., Schwab, J., Siddans, R., Smale, D., Steinbacher, M., Tanimoto, H., Tarasick, D. W., Thouret, V., Thompson, A. M., Trickl, T., Weatherhead, E., Wespes, C., Worden, H. M., Vigouroux, C., Xu, X., Zeng, G., and Ziemke, J.: Tropospheric Ozone Assessment Report: Present-day distribution and trends of tropospheric ozone relevant to climate and global atmospheric chemistry model evaluation, *Elem. Sci. Anth.*, 6, 39, <https://doi.org/10.1525/elementa.291>, 2018.
- Hersbach, H., Bell, B., Berrisford, P., Horányi, A., Muñoz Sabater, J., Nicolas, J., Radu, R., Schepers, D., Simmons, A., Soci, C., and Dee, D.: ERA5 monthly averaged data on pressure levels from 1979 to present, Copernicus Climate Change Service (C3S) Climate Data Store (CDS), <https://doi.org/10.24381/cds.6860a573>, 2019.
- Heue, K.-P., Coldewey-Egbers, M., Delcloo, A., Lerot, C., Loyola, D., Valks, P., and van Roozendaal, M.: Trends of tropical tropospheric ozone from 20 years of European satellite measurements and

- perspectives for the Sentinel-5 Precursor, *Atmos. Meas. Tech.*, 9, 5037–5051, [www.atmos-meas-tech.net/9/5037/2016/](http://www.atmos-meas-tech.net/9/5037/2016/) doi:10.5194/amt-9-5037-2016, 2016.
- Hubert, D., Heue, K.-P., Lambert, J.-C., Verhoelst, T., Allaart, M., Compernelle, S., Cullis, P.D., Dehn, A., Félix, C., Johnson, B.J., Keppens, A., Kollonige, D.E., Lerot, C., Loyola, D., Maata, M., Mitro, S., Mohamad, M., PETERS, A., Romahn, F., Selkirk, H.B., da Silva, F.R., Stauffer, R.M., Thompson, A.M., Veeffkind, J.P., Vömel, H., Witte, J.C., and Zehner, C.: TROPOMI tropospheric ozone column data: geophysical assessment and comparison to ozonesondes, GOME-2B and OMI, *Atmos. Meas. Tech.*, 14, 7405–7433, doi:10.5194/amt-14-7405-2021, 2021.
- IPCC, *Climate Change 2021: The Physical Science Basis. Contribution of Working Group I to the Sixth Assessment Report of the Intergovernmental Panel on Climate Change* [Masson-Delmotte, V., P. Zhai, A. Pirani, S.L. Connors, C. Péan, S. Berger, N. Caud, Y. Chen, L. Goldfarb, M.I. Gomis, M. Huang, K. Leitzell, E. Lonnoy, J.B.R. Matthews, T.K. Maycock, T. Waterfield, O. Yelekçi, R. Yu, and B. Zhou (eds.)]. Cambridge University Press, Cambridge, United Kingdom and New York, NY, USA, <https://www.ipcc.ch/report/ar6/wg1/>, 2021.
- Jöckel, P., Tost, H., Pozzer, A., Kunze, M., Kirner, O., Brenninkmeijer, C. A. M., Brinkop, S., Cai, D. S., Dyrhoff, C., Eckstein, J., Frank, F., Garny, H., Gottschaldt, K.-D., Graf, P., Grewe, V., Kerkweg, A., Kern, B., Matthes, S., Mertens, M., Meul, S., Neumaier, M., Nützel, M., Oberländer-Hayn, S., Ruhnke, R., Runde, T., Sander, R., Scharffe, D., and Zahn, A.: Earth System Chemistry integrated Modelling (ESCiMo) with the Modular Earth Submodel System (MESSy) version 2.51, *Geosci. Model Dev.*, 9, 1153–1200, [www.geosci-model-dev.net/9/1153/2016/](http://www.geosci-model-dev.net/9/1153/2016/) doi:10.5194/gmd-9-1153-2016, 2016.
- Pope, R. J., Kerridge, B. J., Siddans, R., Latter, B. G., Chipperfield, M. P., Feng, W., Pimlott, M. A., Dhomse, S. S., Retscher, C., and Rigby, R.: Investigation of spatial and temporal variability in lower tropospheric ozone from RAL Space UV-Vis satellite products, <https://doi.org/10.5194/acp-23-14933-2023>, *Atmos. Chem. Phys.*, 23, 14933–14947, 2023.
- Schultz, M. G., Schröder, S., Lyapina, O., Cooper, O. R., Galbally, I., Petropavlovskikh, I., von Schneidmesser, E., Tanimoto, H., Elshorbany, Y., Naja, M., Seguel, R. J., Dauert, U., Eckhardt, P., Feigenspan, S., Fiebig, M., Hjellbrekke, A.-G., Hong, Y.-D., Kjeld, P. C., Koide, H., Lear, G., Tarasick, D., Ueno, M., Wallasch, M., Baumgardner, D., Chuang, M.-T., Gillett, R., Lee, M., Molloy, S., Moolla, R., Wang, T., Sharps, K., Adame, J. A., Ancellet, G., Apadula, F., Artaxo, P., Barlasina, M. E., Bogucka, M., Bonasoni, P., Chang, L., Colomb, A., CuevasAgulló, E., Cupeiro, M., Degorska, A., Ding, A., Fröhlich, M., Frolova, M., Gadhavi, H., Gheusi, F., Gilge, S., Gonzalez, M. Y., Gros, V., Hamad, S. H., Helmig, D., Henriques, D., Hermansen, O., Holla, R., Hueber, J., Im, U., Jaffe, D. A., Komala, N., Kubistin, D., Lam, K.-S., Laurila, T., Lee, H., Levy, I., Mazzoleni, C., Mazzoleni, L. R., McClure-Begley, A., Mohamad, M., Murovec, M., Navarro-Comas, M., Nicodim, F., Parrish, D., Read, K. A., Reid, N., Ries, L., Saxena, P., Schwab, J. J., Scorgie, Y., Senik, I., Simmonds, P., Sinha, V., Skorokhod, A. I., Spain, G., Spangl, W., Spoor, R., Springston, S. R., Steer, K., Steinbacher, M., Suharguniyawan, E., Torre, P., Trickl, T., Weilli, L., Weller, R., Xiaobin, X., Xue, L., and Zhiqiang, M.: Tropospheric Ozone Assessment Report: Database and metrics data of global surface ozone observations, *Elem. Sci. Anth.*, 5, 58, <https://doi.org/10.1525/elementa.244>, 2017.
- Sofieva, V. F., Szeląg, M., Tamminen, J., Kyrölä, E., Degenstein, D., Roth, C., Zawada, D., Rozanov, A., Arosio, C., Burrows, J.P., Weber, M., Laeng, A., Stiller, G.P., von Clarmann, T., Froidevaux, L., Livesey, N., van Roozendaal, M., and Retscher, C.: Measurement report: regional trends of stratospheric ozone evaluated using the Merged GRIdded Dataset of Ozone Profiles (MEGRIDOP), *Atmos. Chem. Phys.*, 21, 6707–6720, doi:10.5194/acp-21-6707-2021, 2021.

- Sofieva, V. F., Hänninen, R., Sofiev, M., Szélag, M., Lee, H. S., Tamminen, J., and Retscher, C.: Synergy of Using Nadir and Limb Instruments for Tropospheric Ozone Monitoring (SUNLIT), *Atmos. Meas. Tech.*, 15, 3193–3212, <https://doi.org/10.5194/amt-15-3193-2022>, 2022.
- Tarasick, D., Galbally, I. E., Cooper, O. R., Schultz, M. G., Ancellet, G., Leblanc, T., Wallington, T. J., Ziemke, J., Liu, X., Steinbacher, M., Staehelin, J., Vigouroux, C., Hannigan, J. W., García, O., Foret, G., Zanis, P., Weatherhead, E., Petropavlovskikh, I., Worden, H., Osman, M., Liu, J., Chang, K.-L., Gaudel, A., Lin, M., Granados-Muñoz, M., Thompson, A. M., Oltmans, S. J., Cuesta, J., Dufour, G., Thouret, V., Hassler, B., Trickl, T., and Neu, J. L.: Tropospheric Ozone Assessment Report: Tropospheric ozone from 1877 to 2016, observed levels, trends and uncertainties, *Elem. Sci. Anth.*, 7, 39, <https://doi.org/10.1525/elementa.376>, 2019.
- Thompson, A. M., Witte, J. C., Oltmans, S. J., Schmidlin, F. J., Logan, J. A., Fujiwara, M., Kirchhoff, V. W. J. H., Posny, F., Coetzee, G. J. R., Hoegger, B., Kawakami, S., Ogawa, T., Fortuin, J. P. F., and Kelder, H. M.: Southern Hemisphere Additional Ozonesondes (SHADOZ) 1998–2000 tropical ozone climatology 2. Tropospheric variability and the zonal wave-one, *J. Geophys. Res.-Atmos.*, 108, 8241, <https://doi.org/10.1029/2002JD002241>, 2003.
- Wang, H., Lu, X., Jacob, D. J., Cooper, O. R., Chang, K.-L., Li, K., Gao, M., Liu, Y., Sheng, B., Wu, K., Wu, T., Zhang, J., Sauvage, B., Nédélec, P., Blot, R., and Fan, S.: Global tropospheric ozone trends, attributions, and radiative impacts in 1995–2017: an integrated analysis using aircraft (IAGOS) observations, ozonesonde, and multi-decadal chemical model simulations, *Atmos. Chem. Phys.*, 22, 13753–13782, <https://doi.org/10.5194/acp-22-13753-2022>, 2022.
- Weber, M., Arosio, C., Coldewey-Egbers, M., Fioletov, V., Frith, S.M., Wild, J.D., Tourpali, K., Burrows, J.P., and Loyola, D.: Global total ozone recovery trends derived from five merged ozone datasets, *Atmos. Chem. Phys.*, 22, 6843–6859, [doi:10.5194/acp-22-6843-2022](https://doi.org/10.5194/acp-22-6843-2022), 2022.
- WMO, World Meteorological Organization. Scientific Assessment of Ozone Depletion: 2022, GAW Report No. 278, 509 pp.; WMO: Geneva, 2022.
- Ziemke, J. R., Oman, L. D., Strode, S. A., Douglass, A. R., Olsen, M. A., McPeters, R. D., Bhartia, P. K., Froidevaux, L., Labow, G. J., Witte, J. C., Thompson, A. M., Haffner, D. P., Kramarova, N. A., Frith, S. M., Huang, L.-K., Jaross, G. R., Seftor, C. J., Deland, M. T., and Taylor, S. L.: Trends in global tropospheric ozone inferred from a composite record of TOMS/OMI/MLS/OMPS satellite measurements and the MERRA-2 GMI simulation, *Atmos. Chem. Phys.*, 19, 3257–3269, <https://doi.org/10.5194/acp-19-3257-2019>, 2019.